CORRELATION TRANSFER FROM BASAL GANGLIA TO THALAMUS IN PARKINSON'S DISEASE

by

Pamela Reitsma

B.S., University of Maine, 2007

Submitted to the Graduate Faculty of

the Department of Mathematics in partial fulfillment

of the requirements for the degree of

Master of Sciences

University of Pittsburgh

2010

UNIVERSITY OF PITTSBURGH

DEPARTMENT OF MATHEMATICS

This thesis was presented

by

Pamela Reitsma

It was defended on

August 4, 2010

and approved by

Brent Doiron, Department of Mathematics

G. Bard Ermentrout, Department of Mathematics

Jonathan Rubin, Department of Mathematics

Thesis Advisors: Brent Doiron, Department of Mathematics,

Jonathan Rubin, Department of Mathematics

CORRELATION TRANSFER FROM BASAL GANGLIA TO THALAMUS IN PARKINSON'S DISEASE

Pamela Reitsma, M.S.

University of Pittsburgh, 2010

There is much experimental evidence that neurons located in the basal ganglia of parkinsonian primates show increased pairwise correlations, oscillatory activity, and burst rate compared to normal brain activity. Past computational work has suggested that such changes in the firing pattern of neurons in the globus pallidus internus (GPi), the main output nucleus of the basal ganglia, may compromise thalamocortical relay capabilities. To understand how changes in the patterns of basal ganglia activity affect correlation transfer, we study pairs of realistic models of thalamocortical (TC) relay neurons receiving correlated inhibitory input from the GPi, as well as uncorrelated excitatory signals from cortex. We observe that bursty firing patterns such as those seen in the parkinsonian GPi allow for stronger transfer of correlations and higher correlation susceptibility than do firing patterns found under normal conditions. We also show that removing the T-current in the TC neurons does not significantly affect the correlation transfer, despite its pronounced effects on the spiking of the neurons. Oscillatory firing patterns in GPi are shown to affect the time scale at which correlations are best transferred through the system. We obtain the same results using an integrate-and-fire-or-burst (IFB) model of TC neurons as we do with a more realistic conductance-based model of the TC neurons, suggesting that the IFB model is a good reduced model for studying correlation transfer. In a reduced point process model, we derive analytic calculations of the spike count correlation coefficient for the time-inhomogeneous case. The analysis indicates that the rhythms seen in the transfer of correlations at varying time scales are very robust to different levels of spike correlations and rate correlations

between the neurons. It also points to the fact that these rhythms can be seen because of differences in instantaneous spike correlations, even when the long time scale rhythmic modulation of the neurons in identical. Overall, these results show that parkinsonian firing patterns in GPi do indeed affect the way that correlations are transferred to the thalamus.

TABLE OF CONTENTS

LIST OF TABLES

LIST OF FIGURES

1.0 INTRODUCTION

The basal ganglia is a group of segregated subcortical nuclei which are part of a circuit that is essential to our ability to properly perform motor tasks. There is evidence that the role of the basal ganglia in this circuit is to modulate commands that are relayed from cortex through the thalamus [7]. The motor circuit includes "direct" and "indirect" pathways which play different roles in the initiation and and termination of movement [2]. The basic structure of the motor circuit through the basal ganglia is shown in Figure 1, including the substantia nigra pars compacta (SNc), striatum, subthalamic nucleus (STN), and the globus pallidus externus (GPe) and globus pallidus internus (GPi). The striatum and subthalamic nucleus receive excitatory input from the cortex. These inputs are passed through the circuit, eventually leaving the basal ganglia through the GPi, which inhibits thalamocortical (TC) relay neurons in the thalamus.

The loss of dopaminergic connections from the SNc is the primary cause associated with Parkinson's disease. Much research has been dedicated to the study of how this affects the firing patterns of the basal ganglia. Hallmarks of the parkinsonian basal ganglia are oscillatory firing patterns [3, 7, 9, 12, 19, 21, 28, 29] and an increased burst rate [19, 29]. Specifically, it has been found that there is an increase in the rate of oscillatory bursts in the GPi of monkeys treated with 1-methyl-4-phenyl-1,2,3,6-tetrahydropyridine (MPTP), which induces a parkinsonian state [28, 29]. Computational studies have suggested that these changes in the firing pattern of neurons in the basal ganglia can compromise thalamocortical relay capabilities [10, 24].

One possible reason for this disruption is that oscillatory inhibition would preferentially activate the T-current in the TC neurons, causing these neurons to fire bursts at an elevated rate. However, some experimental evidence has suggested that the TC neurons do not

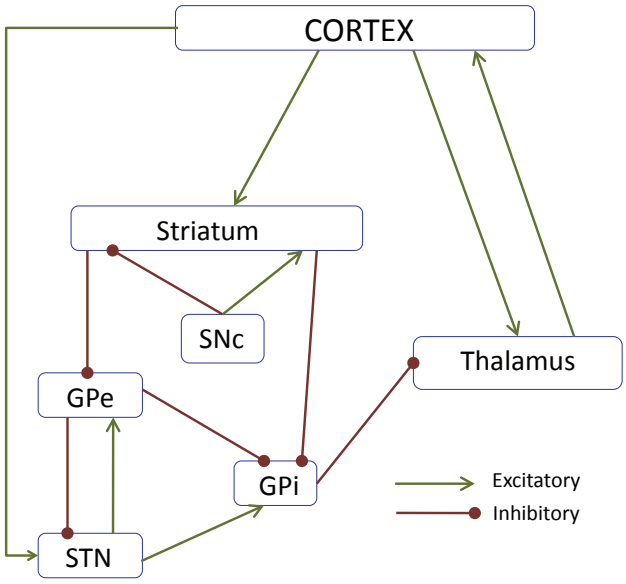

Figure 1: **Motor circuit through basal ganglia.** GPe - globus pallidus externus; GPi - globus pallidus internus; SNc - substantia nigra pars compacta; STN - subthalamic nucleus.

show an increased number of T-current bursts in monkeys treated with MPTP [19]. It is worth noting that this particular study excluded periods of tremor from its analysis, so it is inconclusive about the presence of T-current bursts during tremor, and the possibility that they could contribute to the disruption of thalamocortical relay during these periods.

Several experimental studies have provided evidence for the view that the basal ganglia is a collection of circuits that function in parallel under normal conditions, but that this segregation is broken down in parkinsonism [19]. Specifically, many studies have shown that GPi population neuronal outputs exhibit significant correlations in non-human primates treated with MPTP [3, 12, 18, 21] and in humans with Parkinson's disease [7]. However, the effects of such a break-down in segregation have yet to be investigated computationally.

In this work we investigate how shared changes in firing pattern in the basal ganglia affect the transfer of correlations from GPi to thalamus. We do this by modeling two thalamic neurons, and showing how various firing patterns in correlated GPi inputs affect the transfer of correlation to the model neuron outputs. We begin by discussing two computational

models in Chapter 2. The first is a conductance-based, Hodgkin-Huxley style model, which realistically captures many of the dynamics seen in TC neurons, including T-current bursting [10, 24]. We then study a reduced integrate-and-fire-or-burst (IFB) model which has been shown to reproduce many of the firing patterns observed experimentally [26]. We introduce the ideas of spike count correlations and correlation susceptibility, and discuss how various GPi firing patterns affect the transfer of correlations to thalamus. Then, in Chapter 3, we study a minimal point process model which considers firing of a neuron as escape from an energy well, and show that this minimal model is sufficient to capture some of the important trends in correlation transfer seen in the computational models. In particular, we show analytically how oscillatory firing in GPi affects the transfer of correlation at varying time scales, and how the frequency of this oscillation determines the time scale at which correlation transfer is maximized. Previous studies have shown that in a simple system, correlation has a monotonic relationship to the time scale on which correlations are measured [15]. We show that by taking rhythmic assumptions that describe a parkinsonian state, it is in fact possible to obtain scenarios in which the correlations passed through the system no longer have a monotonic relationship with the observation time scale.

2.0 COMPUTATIONAL MODELS

2.1 DERIVATION OF THE MODELS

In order to investigate how correlations are transferred to the thalamus, we model two identical TC neurons. These neurons receive independent excitatory input from cortex in the form of Poisson spike trains with a rate of $\mu = 20\ Hz$. They also receive inhibitory input from the GPi in the form of time inhomogeneous, Poisson spike trains, with time-dependent rate $\lambda(t)$. These spike trains share a proportion, c, of their spikes. Figure 2 shows the general set-up of connectivity for our model.

The correlated spike trains are generated by first creating a "mother" spike train with rate $\frac{\lambda(t)}{c}$. Then each individual spike is sent independently to each of two "daughter" spike trains with probability c. This results in two spike trains, each with rate λ, which share a fraction, c, of their spikes. Note that for homogeneous poisson spike trains, c is the correlation coefficient, however, for inhomogeneous spike trains, this does not have to be the case, due to the fact that the two spike trains share the same time-dependent rate, $\lambda(t)$. We use four different patterns for $\lambda(t)$, which are shown in Figure 3, and explained in more detail below.

First, we use a Poisson spike train with fixed rate of 70 spikes per second which we characterize as "normal". The firing rate matches experiments [21, 23, 29], and it lacks the dynamic structure seen in GPi spike trains under parkinsonian conditions, which are not seen in non-parkinsonian conditions.

Second, we use an inhomogeneous Poisson spike train with a continuous, periodic rate, and call this the "oscillatory" case. The rate is constructed by summing up 21 weighted sine waves, each with a random phase chosen uniformly from between 0 and 2π. For the oscillatory case shown in Figure 3, the sine waves are shifted up so that the firing rate is centered at 80

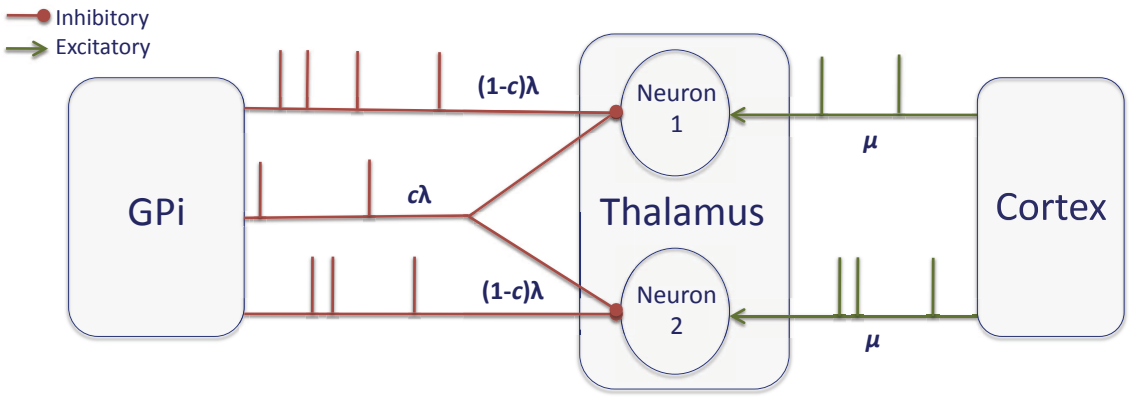

Figure 2: **Diagram of the connectivity and inputs used for the computational models.**

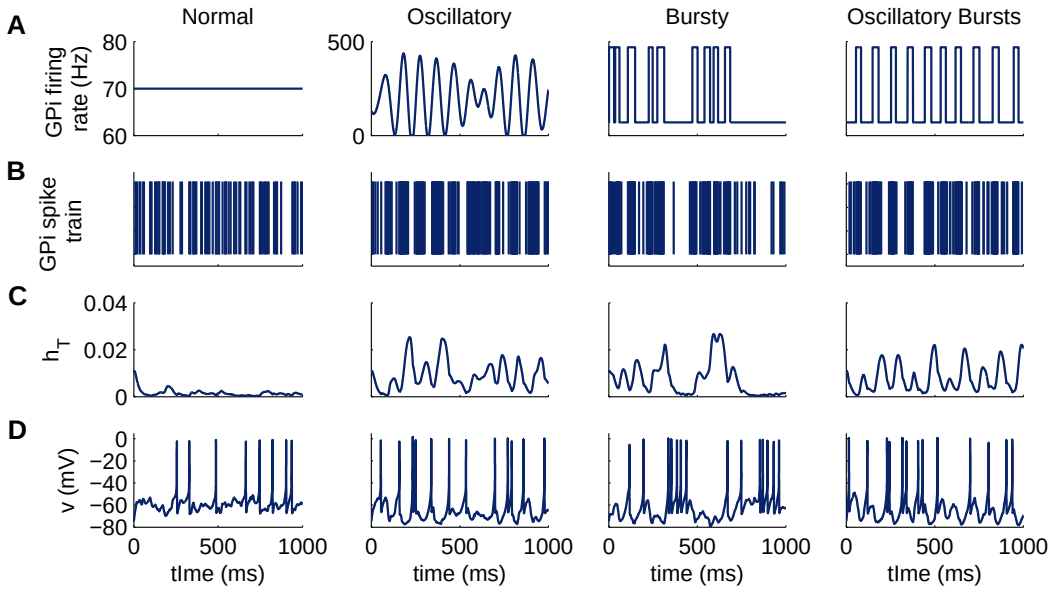

Figure 3: **Example behaviors for each of the four types of input: normal, bursty, oscillatory, and oscillatory bursts. A.** Sample GPi firing rates **B.** Corresponding example of GPi spike trains. **C.** T-current inactivation gate, h_T for the conductance based thalamic model. **D.** Spike train of conductance-based thalamic model neuron in response to 20 Hz excitatory input in addition to the inhibitory input shown above.

spikes per second, and each individual sine wave has a height of 26 spikes per second. If the firing rate ever goes below 0, we simply set it equal to zero. The frequencies of the sine waves vary from 5 to 15 Hz, and the weights are chosen from a gaussian distribution centered at 10 Hz with variance 1.5 Hz. This particular distribution of sine waves was chosen to match the power spectrum of this spike train to power spectra from data taken from oscillatory neurons in the parkinsonian GPi [12].

The third firing pattern is the "bursty" spike train. In this case, the GPi neurons have a discontinuous rate function. Here the baseline firing rate of 70 spikes per second has Poisson distributed bursts of spikes added to it. The firing within each burst is Poisson, and in Figure 3 has a rate of 470 spikes per second. Each burst period is short, and burst duration is taken from a Gaussian distribution. In Figure 3, bursts last a mean time of 30 ms, with a variance of 10 ms, and the mean waiting time between bursts is 70 ms. The overall mean GPi firing rate in this case is 190 spikes per second.

The final firing pattern used is the "rhythmically bursty" spike train. In this case the bursts are constructed in the same way as above, with burst duration taken from the same gaussian distribution and poisson firing at a rate of 470 ms within the bursts. The difference between this and the bursty case is that the waiting time between the bursts is taken from a Gaussian distribution, here with a mean of 70 ms and a variance of 30 ms. Again, the baseline firing rate for this case is 70 spikes per second.

Each of the last three cases are representative of conditions that have been observed experimentally [29]. The parameters used for the spike rates, oscillation frequency, and bursting statistics in Figure 3 are the same parameters used for the conductance based model's GPi inputs for the remainder of the text, unless otherwise specified.

2.1.1 Conductance-Based Model

In this model, the thalamic neurons are described using Hodgkin-Huxley-style equations [13] in which the spiking currents and other currents depend on a conductance and a reversal potential. The model used here is a slight modification of a previously developed model of

TC neurons [10, 24]:

$$Cv' = I_{\text{app}} - I_{\text{leak}} - I_K - I_{Na} - I_T - I_{\text{inhib}} - I_{\text{excite}} \tag{2.1}$$

$$h' = \frac{h_\infty(v) - h}{\tau_h(v)} \tag{2.2}$$

$$h'_T = q_{h_T} \frac{h_{T_\infty}(v) - h_T}{\tau_{h_T}(v)}. \tag{2.3}$$

Here, C is the capacitance, v is a dynamic variable for the membrane potential of a thalamic neuron, and the right-hand-side of Equation 2.1 gives all of the different ionic currents that affect this membrane potential. The first term, I_{app}, is constant current that determines the resting membrane potential. We always choose a value for I_{app} that causes the neuron to be silent in the absence of fluctuations in the synaptic inputs. Each of the other currents are voltage-dependent, and include the parameters $\bar{g}_*$, the maximal conductance of that channel population, and E_*, the reversal potential of the channels. The first voltage-dependent current is the leak current, which is a generic ion current given by $I_{\text{leak}} = \bar{g}_{\text{leak}}(v - E_{\text{leak}})$.

The next two currents in Equation 2.1 are the spiking currents in the model. They are slightly modified from the traditional Hodgkin-Huxley style. The fast activating and slower inactivating sodium current that is responsible for the rising phase of the action potential is given by $I_{Na} = \bar{g}_{Na} m^3 h(v - E_{Na})$. Because the activation is fast, we approximate m by its voltage-dependent steady state value, $m_\infty(v) = 1/\left(1 + \exp\left(-\frac{v+37}{7}\right)\right)$. The sodium inactivation gate, h, is governed by Equation 2.2, with steady state value $h_\infty(v) = 1/\left(1 + \exp\left(\frac{v+41}{4}\right)\right)$, and time constant $\tau_h(v) = \frac{1}{a_h(v)+b_h(v)}$, where $a_h(v) = .128\exp\left(-\frac{46+v}{18}\right)$, $b_h(v) = 4/\left(1 + \exp\left(-\frac{23+v}{5}\right)\right)$.

The slower activating and non-inactivating potassium current is $I_K = \bar{g}_K n^4(v - E_K)$. We let $n = .75(1 - h)$, which is a standard approximation for the activation gate of potassium in terms of the sodium channel inactivation gate [22]. This is a reasonable approximation, since the inactivation of sodium and the activation of potassium both occur on slow time scales that are approximately the same.

The equation $I_T = \bar{g}_T m_T^2 h_T(V - E_{Ca})$ describes the T-current. This depolarizing calcium current allows the TC neurons to fire their characteristic T-current bursts. These bursts

require the neuron to first be hyperpolarized for a sufficiently long time to deinactivate the current, followed by rapid depolarization to allow the current to activate. Because the activation gate, m_T, is fast, we approximate it by $m_{T_\infty}(v) = 1/\left(1+\exp\left(-\frac{v+60}{6.2}\right)\right)$. The dynamics of the slower inactivation gate, h_T, are governed by Equation 2.3, with steady-state value $h_{T_\infty}(v) = 1/\left(1+\exp\left(\frac{v+88}{4}\right)\right)$ and time constant $\tau_{h_T}(v) = 28+\exp\left(-\frac{v+25}{10.5}\right)$.

The remaining two currents model inhibitory inputs from GPi and excitatory inputs from cortex, respectively. The inhibitory synaptic current has the form $I_{\text{inhib}} = \bar{g}_i s_i(v-E_i)$. Here, s_i represents the synaptic filtering of the Poisson spike trains from GPi. For a given GPi spike train, $y(t) = \sum_{k=1}^{n}\delta(t-t_k)$, the synaptic gating is determined by the solution to $\tau_i s_i' = -s_i + y(t)$, with initial condition $s_i(0) = 0$. Similarly, the excitatory input current has the form $I_{\text{excite}} = \bar{g}_e s_e(v-E_e)$ where $\tau_e s_e' = -s_e + x(t)$, $s_e(0) = 0$, for cortical spike train $x(t) = \sum_{j=1}^{m}\delta(t-t_j)$.

The parameters for the conductance based model are given in Table 1. Note that some of the parameters are different than those used in [10] or [24]. In particular, we raised E_{Ca} to reflect the reversal potential of calcium. Also, we raised E_K and lowered g_T to tune the model so that the hyperpolarization phase of the action potential is not sufficient to activate the T-current to such an extent that repetitive firing results. This is because we want firing to be a result of the fluctuations in the inputs, rather than being a self-sustaining process. We also made sure however, that the T-current was still strong enough to cause post-inhibitory rebound bursting after sufficiently long periods of hyperpolarization. Because of the sigmoidal shape of the T-current activation and inactivation curves, the T-current is never completely "off" in this model, so the current makes the neuron more prone to spiking even in the absence of strong inhibition.

2.1.2 Integrate-and-fire-or-burst Model

The integrate-and-fire-or-burst (IFB) model was proposed by Smith and colleagues as a simpler model that is still able to capture the essential dynamics of a TC neuron's spike and burst responses [26]. Here we rederive the model, and detail the changes we made.

Table 1: Parameter values for the conductance-based model and the IFB model.

Parameter	Conductance-Based Model	IFB Model	Units
C	1	2	$\mu F/cm^2$
I_{app}	1.05	.89	nA/cm^2
$\bar{g}_{leak}$	.05	.035	mS/cm^2
$\bar{g}_{Na}$	3	–	mS/cm^2
$\bar{g}_K$	5	–	mS/cm^2
$\bar{g}_T$	2	.07	mS/cm^2
$\bar{g}_{\text{inhib}}$	.024	.024	mS/cm^2
$\bar{g}_{\text{excite}}$	.02	.06	mS/cm^2
E_{leak}	-70	-65	mV
E_{Na}	50	–	mV
E_K	-80	–	mV
E_{Ca}	120	120	mV
E_{excite}	0	0	mV
E_{inhib}	-85	-85	mV
v_h	–	-70	mV
v_{thresh}	–	-50	mV
v_{reset}	–	-68	mV
q_{h_T}	2.5	–	–
τ_h^-	–	20	ms
τ_h^+	–	100	ms
τ_{inhib}	15	15	ms
τ_{excite}	8	4	ms

Each thalamic IFB neuron is governed by the following equations:

$$Cv' = I_{\text{app}} - I_{\text{leak}} - I_T - I_{\text{inhib}} - I_{\text{excite}} \tag{2.4}$$

$$h_T' = \begin{cases} \frac{-h_T}{\tau_h^-} & (v > v_h) \\ \frac{(1-h_T)}{\tau_h^+} & (v \leq v_h) \end{cases} \tag{2.5}$$

As in the conductance based model, C is the capacitance, v is the membrane potential, I_{app} is a constant applied current, $I_{\text{leak}} = \bar{g}_{\text{leak}}(v - E_{\text{leak}})$ is the leak current, and the parameters $\bar{g}_*$ and E_* represent the maximal conductances and the reversal potentials of the various channels, respectively. Like the standard leaky-integrate-and-fire (LIF) model, when v reaches v_{thresh}, a spike is counted and v is instantaneously reset to v_{reset} and held there for a refractory period of 5 ms.

The main difference between this and the standard LIF model is the presence of a current due to T-type calcium channels, $I_T = g_T h_T H[v - v_h](v - E_T)$. The T-current has inactivation variable h_T, which begins to slowly deinactivate when the membrane potential is hyperpolarized below v_h with timescale τ_h^+. If the neuron is then depolarized to above v_h, the T-current immediately activates because of the Heaviside function, $H[v - v_h]$, and h_T begins to inactivate the T-current with timescale τ_h^-. The synaptic currents, I_{excite} and I_{inhib} in the IFB model are constructed in exactly the same way as in the conductance-based model, and have the same physiological interpretations.

The parameters used to simulate the model are given in Table 1. These are different than those used in Smith et. al. [26], and were chosen so that the dynamics of the model would match the dynamics seen in the conductance based model. In particular, we lowered v_{reset} to be below v_{rest} so that the neuron would experience a brief period of hyperpolarization after a spike, and consequently also lowered v_h so that the after-hyperpolarization phase of spiking would not deinactivate the T-current. We also lowered v_{thresh}, and lowered the effective rest potential by using smaller values of injected current. It is worth noting that even without these parameter changes, the trends in correlation transfer in the IFB model are the same as those in the conductance-based model, so the results are robust to changes in parameters.

2.2 SINGLE NEURON PROPERTIES

In this section we discuss the properties of a single TC neuron modeled by the conductance-based model and the IFB model. We consider how GPi firing patterns affect the inter-spike-interval (ISI) distribution, the power spectrum, and the spike triggered averages (STAs).

For each of the firing patterns used in the the conductance-based model in this section, we use the same GPi firing rates, oscillation frequency, and burst statistics as we described in Section 2.1 for Figure 3. The firing rates of the conductance-based model TC neurons for these parameters are 10.6 spikes per second for the normal and oscillatory inputs, and 8.6 spikes per second for the bursty and rhythmically bursty inputs. The bursty inputs produce a lower thalamic firing rate here because the rebound T-current bursts in the thalamic neurons are not sufficient to make up for the periods of very little spiking during the bursts of inhibition in the inputs. There is some experimental evidence that increased inhibition from GPi does indeed cause lower thalamic firing rates in patients with Parkinson's disease compared to other patient populations [17].

For the IFB model, we use the same oscillation frequencies and burst statistics as for the conductance-based model. We also use the same GPi firing rate for the normal condition, but for the bursty and rhythmically bursty cases, the firing within the bursts is at 440 spikes per second as opposed to 470 spikes per second. Also, for the oscillatory case, we center the sine waves at 75 spikes per second instead of 80 spikes per second, and the amplitude of each of the sine waves is 25 spikes per second as opposed to 26 spikes per second. The TC neuron firing rates are around 6.5 spikes per second in the IFB model, which is lower than in the conductance-based model. The lower firing rate is because we chose the firing rate parameters in both models so that the mean input current would not be high enough to cause the neurons to spontaneously fire without fluctuations. In other words, if we set I_{app} to the mean value of the total input currents ($I_{\text{app}} + I_{\text{inhib}} + I_{\text{excite}}$) and then set $\bar{g}_i$ and $\bar{g}_e$ to zero, the neuron would not fire. Thus it is the fluctuations in input spike time arrival that causes the thalamic model neurons to fire. Changing the inputs in the IFB model to allow a higher rate of spiking would have violated this condition.

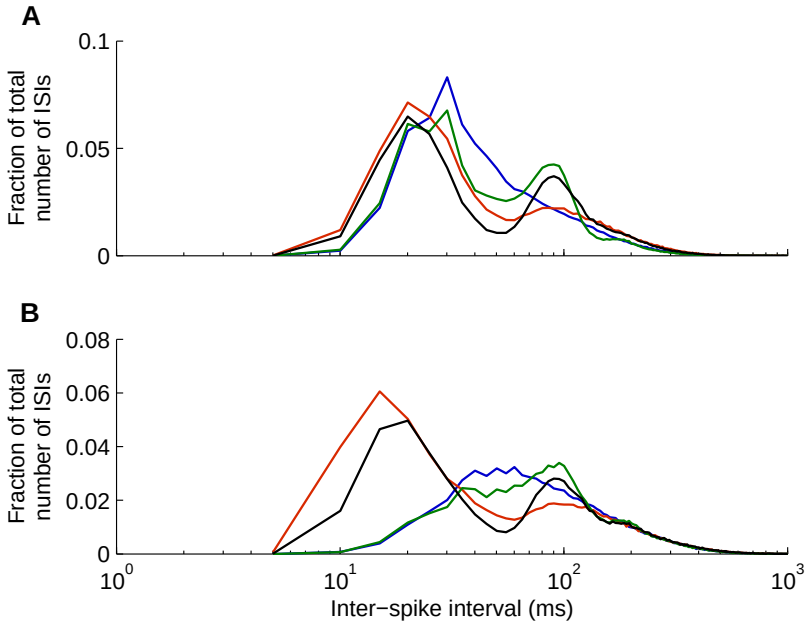

Figure 4: **Thalamic neuron inter-spike interval (ISI) distributions A.** Conductance-based model **B.** IFB model. Normal (blue), oscillatory (green), bursty (red), and rhythmically bursty (black) patterns of GPi inputs are shown.

2.2.1 Inter-Spike Interval (ISI) Distributions

The ISI distributions of our model thalamic neurons are different for each of the different GPi firing patterns used as illustrated in Figure 4. The normal, constant rate inputs from GPi lead to an ISI distribution with a single peak, while both oscillatory firing and oscillatory bursts in GPi lead to a bimodal thalamic ISI distribution. The primary peak (around 30 ms in the normal case of the conductance-based model) is due to the intrinsic firing properties of the neuron. The secondary peak in the cases of oscillatory inhibitory input patterns is because these inputs cause the thalamic neuron to preferentially fire at the period of the oscillation. In this case, the input oscillations are 10 Hz, so the second peak emerges at 100 ms.

Also notable is the fact that the bursty GPi firing patterns, whether oscillatory or not, cause the primary peak of the thalamic ISI distribution to shift to the left when compared to

normal. This indicates that these conditions in the inhibitory inputs are inducing T-current bursts in the TC neurons. These T-current bursts appear when an influx of inhibition causing the neuron to hyperpolarize is followed by a quick release from inhibition which allows the T-current to activate and cause a burst of spikes. Shortening the bursts in GPi would cause the primary peak in the thalamic ISI distribution to be less shifted to the left, because the periods of high inhibition would not be long enough for the T-current to sufficiently deinactivate.

The position of the primary peaks of the ISI distributions in the conductance-based model and the IFB model are slightly different, with the IFB model exhibiting longer ISI's when it receives normal GPi inputs. This is due to the fact that in the absence of a driving signal, the intrinsic firing properties of the two models are different.

2.2.2 Power Spectra

The power spectrum of a spike train is the Fourier transform of the auto-correlation function [8]. It is often used as an indication of how oscillatory the spike train is and gives information about the frequency of oscillations. Figure 5 A shows the power spectra of the spike trains from GPi, and of the spike trains from each of the two thalamic models receiving those inputs. The power spectra for the output spikes were calculated using the Chronux software package [1, 16].

Note that in GPi, both the oscillatory case (green), and the oscillatory bursts (black) show a 10 Hz peak. As mentioned previously, the power spectrum of the oscillatory GPi spike train is a good match to power spectra calculated from recordings in GPi under parkinsonian conditions [12]. Looking at the spectra from the two thalamic models, we see that the spectral peaks in the two rhythmic cases are passed on to the power spectra of the thalamic neurons, as expected.

It is also interesting to notice that the power spectrum of the bursty (red) GPi spike train shows higher power at low frequencies, but no distinct peak. However, these inputs cause the thalamic power spectrum to have a peak around 7 Hz in both the conductance-based model and the IFB model. When the T-current is removed from the models by setting $\bar{g}_T = 0$,

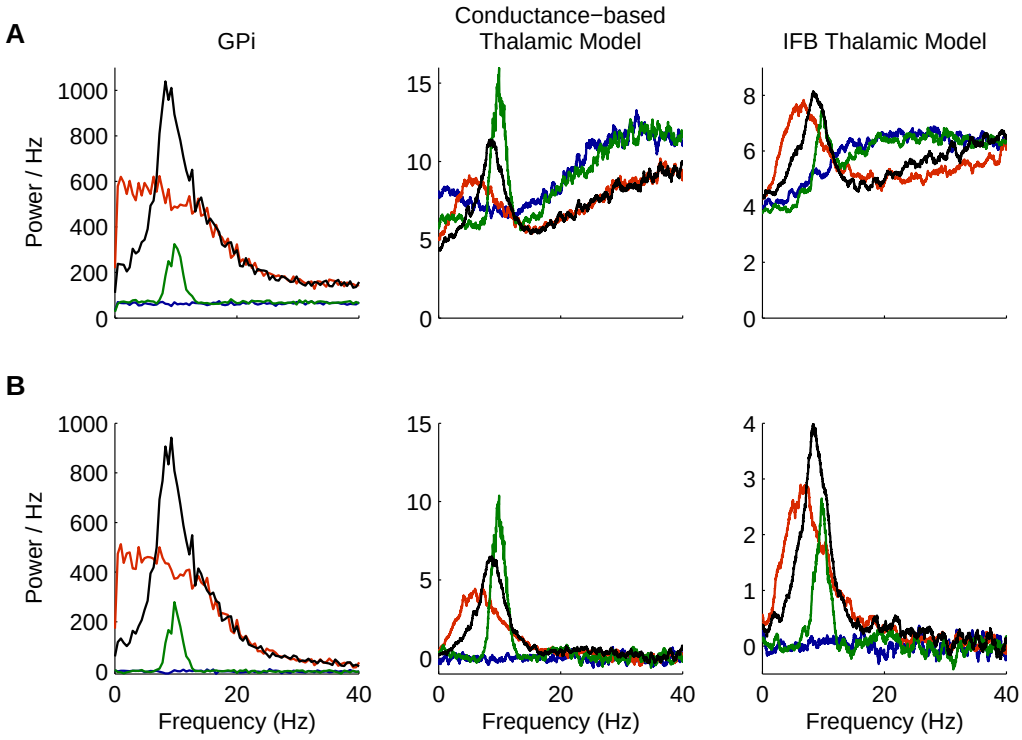

Figure 5: **Power spectra and cross-spectra of GPi and thalamic spike trains. A.** Spike train power spectra **B.** Spike train cross-spectra. The GPi firing patterns are normal (blue), oscillatory (green), bursty (red), and oscillatory bursts (black).

this peak in the thalamic neuron power spectrum disappears for both models. This indicates that the model neurons are frequency selective, and that it is the T-current which is causing them to have this preferred driving frequency.

2.2.3 Spike-triggered Averages

The spike-triggered average (STA) is the average synaptic activity that leads up to the spiking of a neuron [5]. The inputs used in Figure 6 are the total conductances for the inhibitory input, $\bar{g}_i s_i$, (left) and the excitatory input, $\bar{g}_e s_e$ (right). The spike-triggered averages for both of the TC neuron models are shown for each of the different input conditions. The most notable difference is that all conditions except for the normal condition show a peak in the average inhibitory input about 50 ms before a spike. This could be due to a combination of two effects. First, the period of the oscillation in the rhythmic inputs from GPi is 100 ms, so that if spikes tend to occur when inhibition is at its minimum, it makes sense that its maximum is 50 ms earlier. The other possible reason for this peak of inhibition is that the T-current is contributing to spiking. It is clear that the T-current must at least be contributing to spikes in the case of non-oscillatory bursty GPi activity, because this case shows a peak in average inhibition before spikes despite the fact that the input is not rhythmic.

The excitatory input STAs show that the normal and purely oscillatory conditions rely more on the excitation to cause the neuron to spike than the bursty conditions do, as the peak of the average excitation before a spike is highest for these cases. This is another indication that the T-current is helping the neuron to spike more in the cases of bursty inputs than in the non-bursty cases.

The STAs are very similar in the IFB and the conductance-based model, with a few differences. One is that the peak of the excitatory input conductance in the conductance-based model comes slightly before the spike, while in the IFB model it comes at the same time as the spike. This is because the conductance-based model has spiking currents which carry the neuron into spiking once it approaches threshold, while the IFB model has no such spiking currents, so the excitatory input is responsible for pushing the membrane potential all the way across the threshold. The second difference is in the STA of the inhibitory

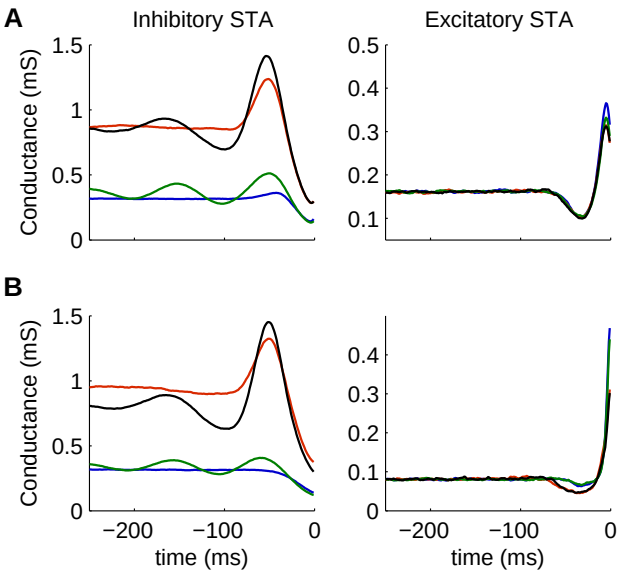

Figure 6: **Spike triggered averages. A.** Conductance-based model **B.** IFB model. The average inhibitory (left) and excitatory (right) input conductances are shown for each of the considered GPi firing patterns: normal (blue), oscillatory (green), bursty (red), and oscillatory bursts (black).

conductance for the case of normal GPi inputs. In the conductance-based model, there is a very slight peak in the inhibition about 50 ms before the spike, which is not seen in the IFB model. This is because in the conductance-based model the T-current is never fully off because of the nature of the activation and inactivation curves. However, in the IFB model, the threshold for the deinactivation of the T-current is sharp. Thus, if the inhibition is sufficiently weak, the membrane potential will rarely go low enough to allow h_T to become non-zero, and hence the inhibitory inputs will not help the neuron towards spiking.

2.3 CORRELATION TRANSFER

2.3.1 Measuring Correlations

The cross-correlation function and its Fourier transform, the cross-spectrum, are two ways of looking at correlations between two spike trains. Figure 7 plots the autocorrelation (red) and cross-correlation (blue) functions of the conductance-based model TC neurons, for each of the patterns of inputs from GPi with $c = 0$. For each case, the main difference between the auto and cross-correlation functions is that the autocorrelation function has a delta function at zero lag while the cross correlation functions show no delta function because $c = 0$. Another difference is that the autocorrelation functions show suppressed spiking for short time lags due to the refractory period of the neurons, while the cross-correlation functions show no refractory period effects. For larger time lags, however, the oscillations in the autocorrelation and cross-correlation functions are identical for the cases of oscillatory firing and oscillatory bursts in the inputs from GPi, and seen in Figure 7 B and D. This is because the two neurons are receiving inputs with identical rate modulations on slow time scales.

The cross-spectra for $c = 0$ are shown in Figure 5 B for the GPi spike trains and the corresponding thalamic spike trains. The cross-spectra for the neurons that receive normal input from GPi (blue) are always flat, and the power is zero because the inputs to the neurons are not correlated. For each of the other patterns of GPi firing, the cross-spectra are very similar to the power spectra shown in Figure 5 A. The main difference is the fact that in the large frequency limit, the cross-spectra always asymptote to zero, while the power spectra limit to the firing rate.

Although the cross-correlation function and the cross-spectrum can be very informative, there are many other ways to measure correlations between two neurons, each with their own advantages and disadvantages. We choose to focus on the Pearson's correlation coefficient of the spike counts of the neurons. This measure quantifies the tendency of the two spike counts to be linearly related to one another. In order to calculate this correlation coefficient, we first count the spikes in bins of size T ms as illustrated in Figure 8. For each of the

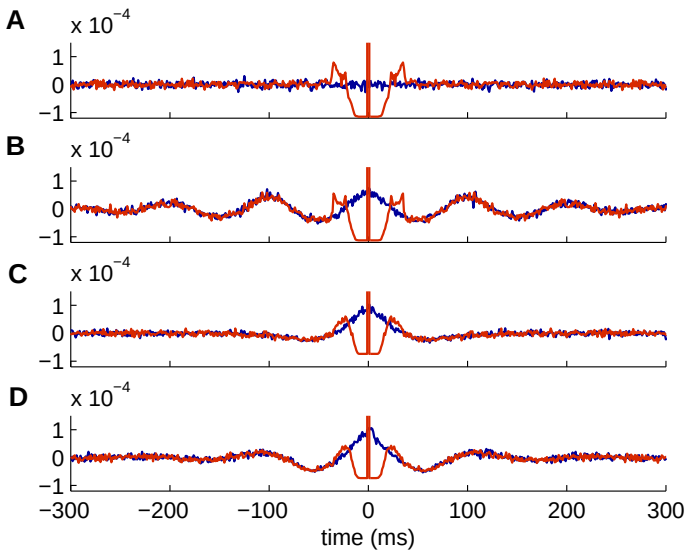

Figure 7: **Correlation functions of the conductance-based model spike trains.** Autocorrelation (red) and cross-correlation (blue) functions with **A.** Normal GPi inputs **B.** Oscillatory GPi inputs **C.** Bursty GPi inputs **D.** Rhythmically bursty GPi inputs.

two neurons, this gives a vector of spike counts, $n_1(T)$ and $n_2(T)$. The Pearson's correlation coefficient is

$$\rho(T) := \frac{\mathrm{cov}(n_1(T), n_2(T))}{\sqrt{\mathrm{var}(n_1(T))\mathrm{var}(n_2(T))}},$$

where $\mathrm{cov}(A, B) = E[AB] - E[A]E[B]$ is the covariance, and $\mathrm{var}(A) = \mathrm{cov}(A, A)$ is the variance.

This correlation coefficient clearly depends on the window size, T, over which the spikes are counted. For T sufficiently small, the two neurons must spike very close together for both to have a spike counted in the same time bin, so in this limit $\rho(T)$ measures synchrony. On the other hand, when T is large, $\rho(T)$ is a measure of correlations at long time scales, and can be thought of as a spike rate correlation. In this case, the exact timing of the spikes makes less of a contribution to the correlations, while co-fluctuations in the firing rates are more important.

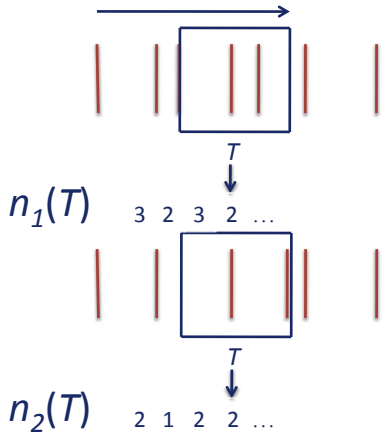

Figure 8: **Spike counts of two spike trains using a sliding window of size T.**

For our model, we can calculate the correlation coefficient of the input spikes from GPi, denoted ρ_{in}, and of the output spikes from thalamus, denoted ρ_{out}. In order to assess how correlation is transferred from GPi to thalamus, we want to compare the input correlation to the output correlation. Figure 9 A plots $\rho_{\text{in}}(95)$ vs. $\rho_{\text{out}}(95)$ for both the conductance-based model and the IFB model. For each pattern of GPi spikes, we let c range between 0 and 1. Note that when $c = 1$, ρ_{out} is still less than 1 because the TC neurons are also receiving independent excitatory input.

It is also interesting to observe that in the cases that the GPi firing is nonhomogeneous, $\rho_{\text{in}} > 0$ even when $c = 0$, because the two GPi spike trains have identical rate modulations. This means that for identical levels of ρ_{in} in the bursty and the normal cases, the cause of the correlations is very different. In the normal case, the correlation comes completely from the spike correlation imposed by c (in fact, $\rho_{\text{in}} = c$), while for the bursty spike trains, the slow, shared rate modulation also contributes to ρ_{in}. With this interpretation, it seems that the spike correlations may be passed on to the outputs more efficiently than the rate correlations. This is evidenced by the fact that as c increases, the ρ_{in} vs ρ_{out} curves for the bursty cases (red and black) cross the curve for the normal case (blue) at ρ_{in}^*. This indicates that when $\rho_{\text{in}} < \rho_{\text{in}}^*$, the correlations in the bursty cases are mostly due to shared

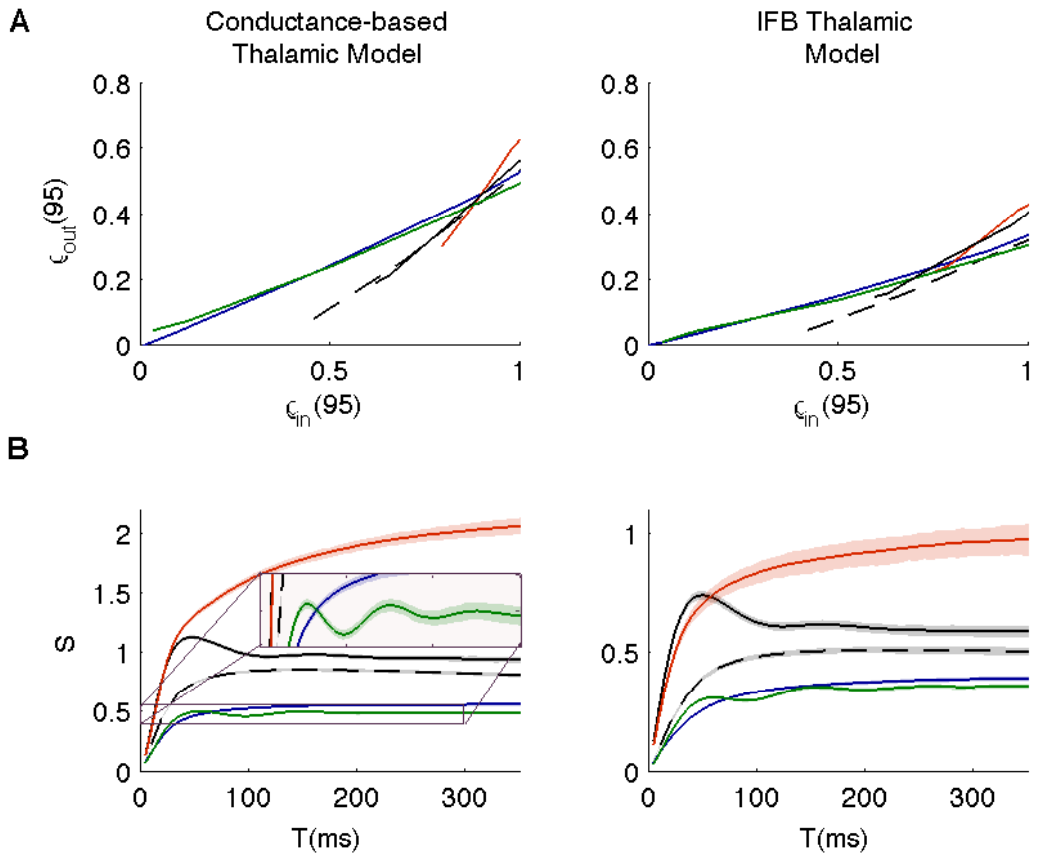

Figure 9: **Input-output correlation relationships and correlation susceptibility. A.** Input correlation vs. output correlation for $T = 95$ ms. **B.** Correlation susceptibility (S) vs. T. The inset shows the oscillations in the susceptibility when the thalamic neurons receive oscillatory inputs. The conductance based model (left), and the IFB model (right) are both shown. The following input conditions are used: normal (blue), oscillatory (green), bursty (red), oscillatory bursts (black). The properties of the oscillatory bursts used for the solid black line are the same as those used in all previous figures, while those used for the dashed black line have a mean time of 330 ms between bursts with a variance of 240 ms. Confidence bands on the correlation susceptibility show 98% confidence, calculated using bootstrapping techniques.

rate fluctuations because c is small, and these correlations are not passed on as efficiently as the spike correlations in the normal case, where c is larger. However, when $\rho_{\text{in}} > \rho_{\text{in}}^*$, c is large enough so that the combination of rate modulation and spike correlations in the bursty cases causes more efficient correlation transfer than do the spike correlations alone in the normal case.

Noticing the fact that the input-output correlation relationship is roughly linear for each of the different firing patterns, we claim that the slope of this curve gives information on the ease of correlation transfer through the system for the observed values of ρ_{in}. Indeed, it has previously been shown that the slope of the input-output correlation curve, called "correlation susceptibility" (denoted S), is a measure of the extent to which small changes in input correlation cause changes in the output correlation [6, 25]. In that work, analytical expressions for this relationship were developed in the case of small input correlations. This is a linear theory, and in a linear system, when the input correlation coefficient is zero, the output correlation coefficient must also be zero, so $\rho_{\text{out}}(T) = S\rho_{\text{in}}(T)$. However, in this work, we define correlation susceptibility in a slightly more relaxed way, because the shared input rate modulation makes it impossible to get $\rho_{\text{in}}(T) = 0$ for nonhomogeneous inputs. Thus, we define the correlation susceptibility as the slope of the attainable portion of the input-output correlation curve, the linearization of which may have a non-zero intercept, $\rho_{\text{out}}(T) = S(T)\rho_{\text{in}}(T) - k$.

Figure 9 B shows the correlation susceptibility, S, plotted as a function of T. We show 98% confidence bands on the correlation susceptibility. These confidence bands were found using a case resampling bootstrapping technique. This technique was applied for each value of T, by taking the set of N pairs $(\rho_{\text{in}}(T), \rho_{\text{out}}(T))$, obtained for every value of c and from every simulation trial run. We ran 30 trials for five different values of c, so $N = 150$. These pairs were then sampled with replacement to obtain a new set of N pairs. This procedure was repeated 1000 times, and the line of best fit was calculated for each constructed data set. The confidence intervals for each value of T are such that 98% of the calculated slopes fall within these intervals.

First, note that the conductance-based model (left) and the IFB model (right) give qualitatively similar results, providing further evidence that the IFB model is a good reduction of

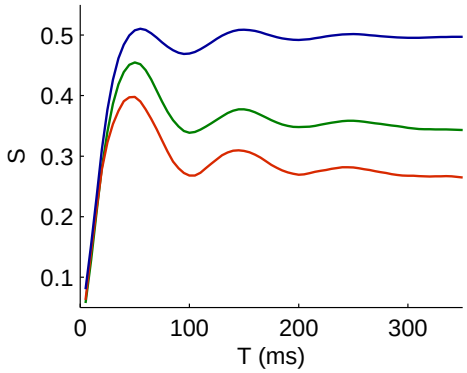

Figure 10: **Susceptibility decreases as oscillation strength increases.** Blue: Mean GPi firing rate= 80 spikes per second, height of sine waves = 26 spikes per second, Green: Mean GPi firing rate= 100 spikes per second, height of sine waves = 57 spikes per second, Red: Mean GPi firing rate= 120 spikes per second, height of sine waves = 85 spikes per second. The conductance-based model is used and in each case the thalamic firing rates are around 10.6 Hz.

the conductance-based model for studying correlation transfer. Also notice that the bursty cases in Figure 9 B have increased correlation susceptibility when compared to the non-bursty cases. This indicates that bursts in GPi cause the system to become more sensitive to small changes in input correlation. This may be due to the fact that bursty inputs provide a strong temporal signal to both neurons. The neurons simultaneously receive periods of strong inhibition, which will cause decreased firing, and then are simultaneously released from the inhibition, causing them to fire at similar times. Thus, even a small change in the input correlation may have a large effect on the output correlation by making the times of firing after the release from inhibition more similar.

One may hypothesize that if the oscillations in the oscillatory case were made stronger to be more comparable to the size of oscillations seen in the bursty cases, that the susceptibility in the oscillatory case would also be increased. However, when the oscillations in the oscillatory case are made stronger while controlling for the input firing rates, the opposite is actually case, with the susceptibility decreasing as the oscillations are made stronger as

shown in Figure 10. Two effects may be causing this difference. The first is that the rate transitions in the bursty cases are sharp, while the rates change more gradually in the oscillatory case. The second possible contribution to this difference is the fact that in the bursty cases, the GPi firing rate never goes below 70 Hz, while the non-bursty oscillatory case has GPi firing rate going as low as zero, and as the oscillation gets stronger, it hits this lower bound more often. Thus, in the periods when the neurons are receiving very little inhibitory input, they are being driven only by their uncorrelated excitatory inputs, which would lower the correlation between the two neurons.

Figure 9 also plots two different patterns of oscillatory bursts. The first (solid black line) uses the same parameters as the oscillatory bursting cases shown in previous plots and given in Section 2.1. The second pattern of oscillatory bursts (dashed black line) is chosen to match data from neurons in GPi showing oscillatory bursty activity [29]. Here, the burst durations have mean 15 ms with variance 5 ms while the time between bursts has a mean of 330 ms and a variance of 240 ms. The GPi firing rate within bursts in still 470 spikes per second for the conductance-based model, and 440 spikes per second for the IFB model, which leads to an overall mean GPi firing rate of 87 spikes per second in the conductance-based model and 86 spikes per second in the IFB model. The thalamic firing rates are 9.9 spikes per second in the conductance-based model and 5.8 spikes per second in the IFB model. Although this new rhythmically bursty case has slightly lower correlation susceptibility than the other, its correlation susceptibility is still higher than that of the non-bursty cases.

As seen most clearly in the inset in Figure 9 B, the correlation susceptibility of the cases with rhythmic firing in the GPi is also rhythmic. The frequency of the oscillation of the correlation susceptibility is the same as that in the inhibitory input from GPi, which in the case shown is 10 Hz. The oscillatory bursts show this same rhythm in correlation susceptibility if the variance of the time between bursts is sufficiently small.

2.3.2 Effects of Parameter Changes on Correlation Transfer

In the following sections, we discuss how changing various characteristics of the different GPi firing patterns affects the transfer of correlations to the TC neurons. Specifically, we look

at the effects of changing the frequency of oscillations and the variance of the waiting time between bursts in the GPi on the correlation susceptibility of the system. We also consider how changing the properties of the thalamic neurons by removing T-current bursts can affect correlation transfer through the system.

2.3.2.1 Varying Frequency It is relevant to ask how changing the frequency of the oscillations in the GPi affects the correlation transfer, since data shows that there is a range of possible GPi oscillation frequencies under Parkinsonian conditions [21, 29]. In Figure 11 A, we change the frequency of the oscillatory bursts by changing the mean waiting time between bursts. Notice that as the mean waiting time between bursts increases, the amplitude of the oscillation in the susceptibility also increases. Increasing the waiting time between bursts, while leaving all other parameters the same causes the thalamic firing rate to increase, which may be part of the reason for this increase in the amplitude of the rhythm in the susceptibility. With a mean time of 70 ms between bursts (blue), the thalamic firing rate is 8.6 spikes per second, for 95 ms between bursts (red) the thalamic firing rate is 9.3 spikes per second and for 136.67 ms between bursts (green), the thalamic firing rate is 9.9 spikes per second. Here, in order to make the rhythms more clear, the variance of the burst time is set to 5 ms, and the variance of the waiting time between bursts is 10 ms, with all other parameters the same as those used in Figure 3 and introduced in Section 2.1.

Figure 11 B shows the effects of changing the frequency of oscillations in the GPi for the non-bursty oscillatory case. Once again, decreasing the frequency of the oscillation causes the rhythm in the susceptibility as a function of T to become stronger. It is also clear that the rhythm in the correlation susceptibility is the same frequency as the rhythm in the GPi firing rate. Again, the TC neuron firing rates increase slightly as the oscillation frequency decreases, with firing rates of 10.6 spikes per second when the oscillation is 10 Hz, 10.9 spikes per second when the oscillation is 8 Hz, and 11.2 spikes per second when the oscillation is 6 Hz.

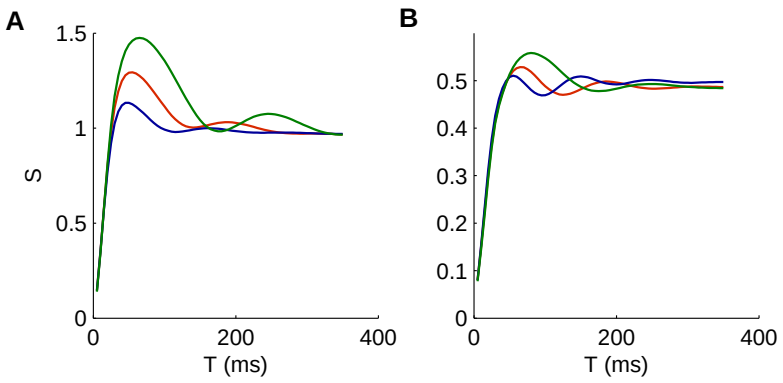

Figure 11: **Oscillation amplitude of S decreases as oscillation frequency in GPi increases.** Frequencies are 10 Hz (blue), 8 Hz (red), 6 Hz (green), for both oscillatory bursts (left) and non-bursty oscillations (right) in the inputs from GPi to the conductance-based thalamic model.

Thus we see that higher frequencies of GPi temporal activity decrease the effect of the oscillations on the correlation transfer. We also observed in Figure 10 that increasing the rate and amplitude of oscillatory inputs causes the correlation susceptibility to decrease. Taken together, these two effects indicate a possible mechanism for the therapeutic effect of deep brain stimulation (DBS). By forcing high frequency rhythms, DBS could decrease correlations that are passed on to the thalamus because of pathologically synchronous firing rate modulations in the basal ganglia.

2.3.2.2 Diluting Oscillations In the oscillatory bursting case, increasing the variance of the waiting time between GPi bursts makes the oscillation in the correlation susceptibility less pronounced, as seen in Figure 12. However, it also raises the correlation susceptibility. This makes sense, since increasing the variance of the time between bursts makes the oscillatory bursting case more similar to the non-oscillatory bursting case, which has higher susceptibility. One possible reason for the increase in S is that when the bursts are non-oscillatory, there is a higher probability that they will arrive with very little time in between. This results in a much longer period of high inhibition to the TC neurons, which will cause

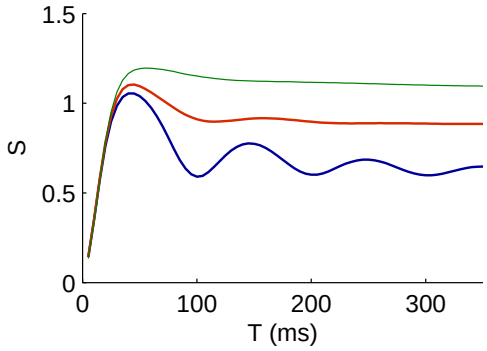

Figure 12: S **increases as variance of time between bursts increases.** Rhythmically bursty GPi inputs to the conductance based model are used with variances of the time between bursts of $10ms$ (blue), $30ms$ (red), and $50ms$ (green).

them both to fire very little during that time. Then when they are simultaneously released from this strong inhibition, they will both tend to fire together and will be very sensitive to small differences in input correlations.

2.3.2.3 Removing T-current Because we have already seen evidence that the T-current plays a role in the spiking of the thalamic neurons that receive bursty input from GPi, it makes sense to investigate how removing this current affects the firing of these neurons and the correlation transfer of the system. When the T-current is removed in the conductance-based model, the firing rate of the thalamic neurons decreases for every input firing pattern we tested. The rates of thalamic firing without the T-current are 7.5 spikes per second for normal inputs from GPi, 6.9 spikes per second for oscillatory inputs, and 2 spikes per second for both rhythmic and non-rhythmic bursty inputs, so removing the T-current clearly does have an effect on the thalamic firing in every case. This decrease in firing rate could be compensated for by increasing I_{app}, however we chose to leave all parameters the same to obtain the most fair comparison.

Figure 13 A shows the STAs for the conductance-based model with (solid) and without (dashed) the T-current. Removing the T-current most strongly affects the STA of the non-

oscillatory bursty case (red), causing the peak in the inhibition before a spike to completely disappear when the T-current is removed. The STAs for the oscillatory cases on the other hand, are not as strongly affected, with the main effect being that the peak in the inhibition shifts to the left, so it occurs longer before the spike. Thus, although removing the T-current in these cases changes the rate of firing, it does not significantly change the average input that causes the neurons to fire.

Despite the drastic change in the STA of neurons with bursty inputs from GPi and the large change in the thalamic firing rates for all input types, the correlation susceptibility is not very strongly affected by the removal of the T-current, as seen in Figure 13 B. This indicates that the T-current is not essential for the patterns of correlation transfer that we see in the system, although it does influence the single neuron firing patterns.

Removing the T-current from the IFB model produces similar results, in that thalamic firing patterns are strongly affected, while correlation susceptibility shows little change. It is worth nothing that without the T-current, the IFB model is simply a leaky-integrate-and-fire (LIF) model. Thus, the level of complexity in an LIF model is sufficient to produce the patterns in correlation transfer seen here. This suggests that perhaps even less complex models could be used to explain such patterns.

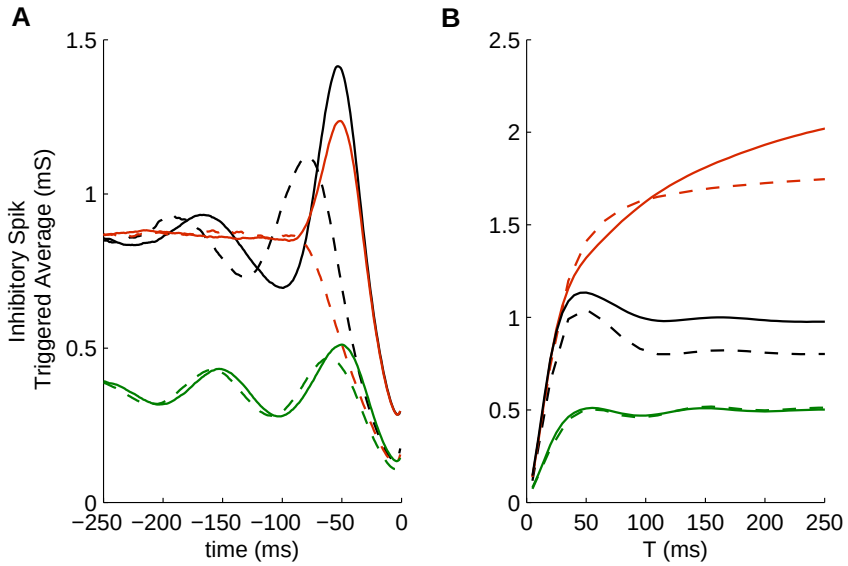

Figure 13: **Removing the T-current (dashed lines) affects spike triggered average, but not correlation susceptibility. A.** Spike triggered averages **B.** Correlation susceptibility. GPi firing patterns used are: oscillatory (green), bursty (red), and oscillatory bursts (black).

3.0 REDUCED MODEL

3.1 MODEL DERIVATION

In order to provide an analytic explanation for the trends that we see in the transfer of correlations under the oscillatory conditions discussed above, we consider a phenomenological model of TC spike activity. In an excitable neuron, we can think of spiking as a process that requires a certain amount of activation energy. The amount of energy required depends on how far the resting potential is below the spiking threshold and on the strength of the inputs it receives. Attaining this activation energy and consequently spiking can be considered as the escape of a diffusive particle from an energy well, the height of which is related to the distance between rest and threshold.

Under the assumption that the well height is large and the diffusion rate of the particle is small, it has been shown that the rate of escape of a particle from the energy well is given by an Arrhenius escape rate [11],

$$\alpha(t) = \beta \exp\left[-\frac{U(t)}{D}\right].$$

Here, D is the rate of diffusion, which depends on the noise strength, and the well height is given by $U(t)$, as long as the temporal variations in $U(t)$ are sufficiently slow.

This Arrhenius escape rate has been shown to be a good approximation to the rate of firing of a neuron in the limit of small input strength (rate of diffusion) and large distance between rest and threshold (well height) [20]. When applying this theory to a neuron, β can be thought of as a free parameter which can be fit to data [20].

In order to apply this theory to our model thalamic neurons, we assume that the synaptic inputs provide the noise necessary to reach threshold. We also assume that the modulations

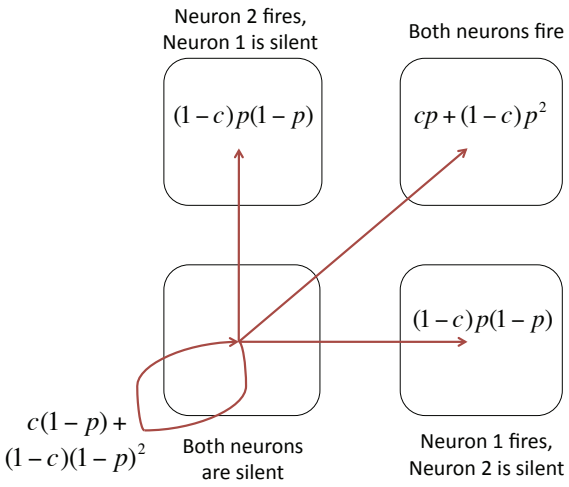

Figure 14: **Joint escape probabilities of two neurons in the interval** $(t, t+dt)$**.** The neurons have spike correlation c, and each has escape probability $p(t)$.

of the inhibitory input rate change the average amount of inhibition over time, which causes the effective resting membrane potential to be time-dependent. We assume that this directly affects the height of the energy well, causing $U(t)$ to be time-dependent.

If we now have two neurons, each with escape rate $\alpha(t)$, we can calculate the joint firing probabilities for the neurons given that the probability of one neuron firing in the interval $(t, t+dt)$ is $p(t) = \alpha(t)dt$. A fraction, c, of the inputs to the two neurons are shared, and we assume the system is linear, so input correlation is equal to output correlation. Thus, when $c = 0$ the neurons are independent, so the probability that both neurons will fire in that interval is $p(t)^2$, and when $c = 1$, the neurons are receiving identical inputs, so the probability of both neurons firing is $p(t)$. For $c \in (0, 1)$, the probability that the neurons fire independently is $1-c$, and the probability that the firing is the same is c, because the input correlation is equal to the output correlation. If the firing is independent, the probability that both neurons will fire is $p(t)^2$, the probability that one neuron will fire while the other does not is $p(t)[1-p(t)]$, and the probability that neither neuron fires is $[1-p(t)]^2$. If the firing is the same, both neurons fire with probability $p(t)$, or both neurons are silent with probability $1-p(t)$. Combining the probabilities for the cases of independent and identical

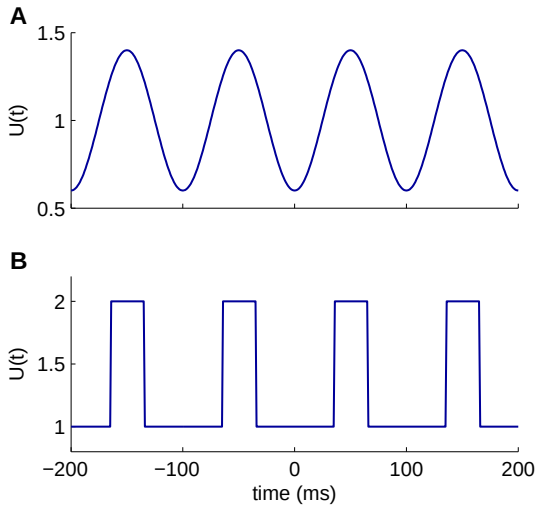

Figure 15: **Modulation of energy well heights.A.** Oscillatory modulation. **B.** Rhythmically bursty modulation.

firing, we have that the total probability of both neurons firing is $cp(t) + (1-c)p(t)^2$, the total probability of neither neuron firing is $c[1-p(t)] + (1-c)[1-p(t)]^2$, and the probability of only one of the neurons firing is $(1-c)p(t)[1-p(t)]$. A schematic outlining the joint probabilities for the firing of two neurons for $c \in [0,1]$ is shown in Figure 14.

To model the well modulation that occurs due to non-bursty, oscillatory, inhibitory inputs with frequency Ω, we let

$$U(t) = U_0 \left(1 - \eta \cos\left(2\pi\Omega t\right)\right). \tag{3.1}$$

Here, U_0 is the average well height and η is the modulation strength. This is simplified from the oscillatory inputs used in the computational models in that the modulation consists of a single sinusoid, rather than a sum of sinusoids. This is the same well height modulation used in Wiesenfeld et. al. [30].

To model the well modulation resulting from oscillatory bursty inputs, we let

$$U(t) = U_0 \left(1 + \eta H\left[t\mathrm{mod}(M) - \frac{T_1}{2}\right] H\left[\frac{T_1}{2} + T_2 - t\mathrm{mod}(M)\right]\right), \tag{3.2}$$

where T_1 is the time between bursts, T_2 is the burst duration, and $M = T_1 + T_2$ is the period of the oscillation. Again, this is a simplification of the oscillatory bursty inputs used in the computational models, because the period of the oscillation in this case is fixed, without any of the jitter that the gaussian distributions of waiting times and burst times introduce in the computational models.

A plot of each of these well heights is shown in Figure 15. Note that we have constructed the well-heights to be even functions to simplify later calculations.

3.2 CALCULATION OF CORRELATION FUNCTIONS

Here we derive the equations for the auto and cross-correlation functions of a poisson spike train with periodic rate, and apply this to the reduced model neurons with the Arrhenius escape rates given in Equations 3.1 and 3.2. For derivations of the auto-correlation function in a more general setting, see [14, 27, 30].

Consider a delta spike train with M-periodic escape rate $\alpha(t)$ and mean escape rate $\nu = \langle \alpha(t) \rangle_t$, where $\langle \cdot \rangle_t$ denotes the time average. Because of the periodicity of the spike train statistics, let $Z(t)$ be the spike train restricted to the interval $t \in (0, M)$. Following the derivation in Van Kampen [27], let $Q_s(t_1, t_2, \ldots, t_s)$ be the probability of having the particular spike train,

$$z(t) = \sum_{n=1}^{s} \delta(t - t_n),$$

which contains s spikes at the times $(t_1, t_2, \ldots, t_s) \in (0, M)$. The probabilities of every possible spike train in this interval, with any possible number of spikes, must add up to 1, so we have the condition,

$$1 = Q_0 + \int_0^M Q_1(t_1) dt_1 + \int_0^M \int_{t_1}^M Q_2(t_1, t_2) dt_2 dt_1 + \cdots,$$

which assumes ordered spike times, $0 < t_1 < t_2 < \cdots < M$. Equivalently, allowing the spike times to be in any order and dividing by the number of possible permutations to correct for

this allowance we have,

$$1 = Q_0 + \sum_{s=1}^{\infty} \frac{1}{s!} \int_0^M \cdots \int_0^M Q_s(t_1, t_2, \ldots, t_s) dt_1 dt_2 \cdots dt_s.$$

Now define functions $f_n(t_1, t_2, \ldots, t_n)$ by

$$f_n(t_1, t_2, \ldots, t_n) = \sum_{s=n}^{\infty} \frac{1}{(s-n)!} \int_0^M \cdots \int_0^M Q_s(t_1, t_2, ...t_n, t'_{n+1}, ...t'_s) dt'_{n+1} \cdots dt'_s. \tag{3.3}$$

Then for $dt_1, dt_2, \ldots, dt_n$ small, $f_n(t_1, t_2, \ldots, t_n) dt_1 dt_2 ... dt_n$ is approximately equal to the probability of having exactly one spike in each of the intervals $(t_1, t_1+dt_1), (t_2, t_2+dt_2), \ldots, (t_n, t_n+dt_n)$, regardless of the number or timing of spikes outside of these intervals.

Averaging across all possible realizations of the spike train gives

$$\begin{aligned} E[Z(t)] &= \left\langle \sum_{n=1}^{s} \delta(t - t_n) \right\rangle \\ &= \sum_{s=1}^{\infty} \frac{1}{s!} \int_0^M \cdots \int_0^M \sum_{n=1}^{s} \delta(t - t_n) Q_s(t_1, t_2, \ldots, t_s) dt_1 dt_2 \cdots dt_s, \end{aligned}$$

which weights every possible spike train by its probability. Here, the average is taken over all possible spike times $(t_1, t_2, ..., t_s)$ for each fixed s, and also over s. This simplifies to

$$E[Z(t)] = \sum_{s=1}^{\infty} \frac{1}{(s-1)!} \int_0^M \cdots \int_0^M \delta(t - t_1) Q_s(t_1, t_2, \ldots, t_s) dt_1 dt_2 \cdots dt_s,$$

because each of the s spikes in a spike train is identical. Plugging in Equation 3.3, we can rewrite this as

$$\begin{aligned} E[Z(t)] &= \int_0^M \delta(t - t_1) f_1(t_1) dt_1 \\ &= f_1(t), \end{aligned}$$

or equivalently,

$$E[Z(t)] = \alpha(t) \tag{3.4}$$

for $t \in (0, M)$, since

$$f_1(t)dt = P[\text{neuron spikes once in } (t, t + dt)] = \alpha(t)dt$$

because the firing is Poisson.

Now let $Y(t) = Z(t) - \nu$ be the zero-average spike train on this interval. Then we can calculate the time-dependent auto-correlation function:

$$\begin{aligned}
E[Y(t+\tau)Y(t)] =& \left\langle \left(\sum_{n=1}^{s} \delta(t+\tau-t_n) - \nu \right) \left(\sum_{n'=1}^{s} \delta(t-t_{n'}) - \nu \right) \right\rangle \\
=& \left\langle \sum_{n=1}^{s} \delta(t+\tau-t_n)\delta(t-t_n) \right\rangle + \left\langle \sum_{\substack{n=1 \\ n\neq n'}}^{s} \sum_{n'=1}^{s} \delta(t+\tau-t_n)\delta(t-t_{n'}) \right\rangle \\
& - \nu \left\langle \sum_{n=1}^{s} \delta(t-t_n) \right\rangle - \nu \left\langle \sum_{n=1}^{s} \delta(t+\tau-t_n) \right\rangle + \nu^2 \\
=& \sum_{s=1}^{\infty} \frac{1}{s!} \int_0^M \cdots \int_0^M \sum_{n=1}^{s} \delta(t+\tau-t_n)\delta(t-t_n) Q_s(t_1, t_2, \ldots, t_s) dt_1 dt_2 \cdots dt_s \\
& + \sum_{s=2}^{\infty} \frac{1}{s!} \int_0^M \cdots \int_0^M \sum_{\substack{n=1 \\ n\neq n'}}^{s} \sum_{n'=1}^{s} \delta(t+\tau-t_n)\delta(t-t_{n'}) Q_s(t_1, t_2, \ldots, t_s) dt_1 dt_2 \cdots dt_s \\
& - \nu E[Z(t)] - \nu E[Z(t+\tau)] + \nu^2,
\end{aligned}$$

where the first two terms weight the product of every possible spike train and its corresponding τ-shifted spike train by the probability of that spike train. Again, the averages are taken over all possible spike train lengths, and over all possible spike times within a train of length s. Plugging in Equation 3.4 and again using the fact that every spike in the spike trains are identical, this simplifies to

$$\begin{aligned}
E[Y(t+\tau)Y(t)] =& \sum_{s=1}^{\infty} \frac{1}{(s-1)!} \int_0^M \delta(t+\tau-t_1)\delta(t-t_1) Q_s(t_1, t_2, \ldots, t_s) dt_1 dt_2 \cdots dt_s \\
& + \sum_{s=2}^{\infty} \frac{1}{(s-2)!} \int_0^M \delta(t+\tau-t_1)\delta(t-t_2) Q_s(t_1, t_2, \ldots, t_s) dt_1 dt_2 \cdots dt_s \\
& - \nu\alpha(t) - \nu\alpha(t+\tau) + \nu^2.
\end{aligned}$$

Plugging in Equation 3.3 gives

$$\begin{aligned}
E[Y(t+\tau)Y(t)] =& \int_0^M \delta(t+\tau-t_1)\delta(t-t_1) f_1(t_1) dt_1 \\
& + \int_0^M \int_0^M \delta(t+\tau-t_1)\delta(t-t_2) f_2(t_1, t_2) dt_1 dt_2 \\
& - \nu\alpha(t) - \nu\alpha(t+\tau) + \nu^2 \\
=& f_1(t)\delta(\tau) + f_2(t+\tau, t) - \nu\alpha(t) - \nu\alpha(t+\tau) + \nu^2,
\end{aligned}$$

which can be rewritten as

$$E[Y(t+\tau)Y(t)] = \alpha(t)\delta(\tau) + f_2(t+\tau,t) - \nu\alpha(t) - \nu\alpha(t+\tau) + \nu^2. \tag{3.5}$$

The periodicity of $\alpha(t)$ implies that $f_2(t+\tau,t)$ can be periodically extended to be defined on $(-\infty,\infty)$, so that Equation 3.5 is defined for all t and all τ.

From Equation 3.5, we can now calculate the time-averaged auto-correlation function of this spike train:

$$\begin{aligned} A(\tau) :=& \frac{1}{M}\int_0^M E[Y(t+\tau)Y(t)]dt \\ =& \frac{1}{M}\int_0^M \left[\alpha(t)\delta(\tau) + f_2(t+\tau,t) - \nu\alpha(t) - \nu\alpha(t+\tau) + \nu^2\right] dt, \end{aligned}$$

Thus,

$$A(\tau) = \nu\delta(\tau) + f_{av}(\tau) - \nu^2, \tag{3.6}$$

where $f_{av}(\tau) = \frac{1}{M}\int_0^M f_2(t+\tau,t)dt$, and we use the fact that since $\alpha(t)$ is M-periodic,

$$\frac{1}{M}\int_0^M \alpha(t)dt = \langle\alpha(t)\rangle_t = \langle\alpha(t+\tau)\rangle_t = \nu.$$

If we assume that the spike trains are Poisson, then the probabilities of spikes in the intervals $(t, t+dt)$ and $(t', t'+dt')$ are independent. Thus,

$$f_2(t,t') = f_1(t)f_1(t') = \alpha(t)\alpha(t') = \alpha(t)\overline{\alpha(t')},$$

with the last equality coming from the fact that firing rates must be real. Also, because we have assumed that $\alpha(t)$ is periodic, we can write it as a complex Fourier series:

$$\alpha(t) = \sum_{n=-\infty}^{\infty} c_n e^{in2\pi\Omega t},$$

where $\Omega = \frac{1}{M}$ is the frequency.

Thus,

$$\begin{aligned}
f_{av}(\tau) =& \frac{1}{M}\int_0^M \alpha(t+\tau)\overline{\alpha(t)}dt \\
=& \frac{1}{M}\int_0^M \sum_{n=-\infty}^{\infty} c_n e^{in2\pi\Omega(t+\tau)} \sum_{n'=-\infty}^{\infty} \overline{c}_{n'} e^{-in'2\pi\Omega t} dt \\
=& \frac{1}{M}\int_0^M \sum_{n=-\infty}^{\infty} |c_n|^2 e^{in2\pi\Omega\tau} dt \\
=& \sum_{n=-\infty}^{\infty} |c_n|^2 e^{in2\pi\Omega\tau} \\
=& |c_0|^2 + 2\sum_{n=1}^{\infty} |c_n|^2 \cos(n2\pi\Omega\tau),
\end{aligned}$$

where the last equality assumes that $\alpha(t)$ is an even function.

Note that since $\alpha(t)$ is an even function, we can also directly write it as the cosine series,

$$\alpha(t) = \alpha_0 + \sum_{n=1}^{\infty} \alpha_n \cos(2\pi n\Omega t). \tag{3.7}$$

The coefficients of cosine in the trigonometric Fourier series are related to the coefficients of the complex Fourier series by $\alpha_0 = c_0$ and $\alpha_n = c_n + c_{-n} = 2\text{Re}(c_n)$ for $n \geq 1$. Thus,

$$f_{av}(\tau) = |\alpha_0|^2 + \frac{1}{2}\sum_{n=1}^{\infty} |\alpha_n|^2 \cos(2\pi n\Omega\tau), \tag{3.8}$$

We directly calculate the coefficients α_j in Appendix A for the two different well height functions, $U(t)$, introduced in Section 3.1, which are both even functions.

From Equation (3.7) it is clear that the mean firing rate of the neuron is $\nu = \alpha_0$ which must be real, so plugging Equation (3.8) into Equation (3.6) and replacing ν by α_0 we have

$$A(\tau) = \alpha_0\delta(\tau) + |\alpha_0|^2 + \frac{1}{2}\sum_{n=1}^{\infty} \alpha_n^2 \cos(2\pi n\Omega\tau) - \alpha_0^2,$$

which simplifies to

$$A(\tau) = \alpha_0\delta(\tau) + \frac{1}{2}\sum_{n=1}^{\infty} |\alpha_n|^2 \cos(2\pi n\Omega\tau),$$

the autocorrelation function of the neuron as given in Wiesenfeld et al, 1994 [30].

Because the two neurons are assumed to be identical, we can extend the autocorrelation function to obtain the cross-correlation function. Because the firing is Poisson, and the two neurons are receiving identical rate modulations, the cross-correlation function should be identical to the auto-correlation function when $\tau \neq 0$. The main difference is that the probability that one neuron will spike in the interval $(t, t+dt)$ is given by $p(t) = \alpha(t)dt$, while the probability that both neurons will spike in this interval is given by

$$\begin{aligned} cp(t) + (1-c)p(t)^2 =& c\alpha(t)dt + (1-c)[\alpha(t)dt]^2 \\ =& c\alpha(t)dt + o(dt) \end{aligned}$$

as is seen by the schematic in Figure 14. Thus the instantaneous joint firing rate is

$$\begin{aligned} \lim_{dt\to 0} \frac{cp(t) + (1-c)p(t)^2}{dt} =& \lim_{dt\to 0} \frac{c\alpha(t)dt + o(dt)}{dt} \\ =& c\alpha(t). \end{aligned}$$

so the mean joint firing rate is $c\alpha_0$.

Using these two facts we deduce that the cross-correlation function is

$$\begin{aligned} C(\tau) =& c\alpha_0\delta(\tau) + f_{av}(\tau) - \alpha_0^2 \\ =& c\alpha_0\delta(\tau) + \frac{1}{2}\sum_{n=1}^{\infty} \alpha_n^2 \cos(2\pi n\Omega\tau). \end{aligned}$$

The height of the delta function is the mean of the joint firing rate of the two neurons. This function shows that for $\tau \neq 0$, the statistics of the firing of the two neurons is identical. This is in agreement with the observation in Section 2.3.1 that the auto and cross-correlation functions of the computational thalamic models with inhibitory inputs that have identical rate modulations are the same for lags sufficiently far from zero. It also matches results obtained by simulating the reduced model and calculating the cross-correlation function numerically.

3.3 CALCULATION OF CORRELATION COEFFICIENT

Beginning with the equations for the autocorrelation and cross-correlation functions introduced in Section 3.2,

$$A(\tau) = \alpha_0\delta(\tau) + \frac{1}{2}\sum_{n=1}^{\infty}\alpha_n^2\cos(n2\pi\Omega\tau) \tag{3.9}$$

and

$$C(\tau) = c\alpha_0\delta(\tau) + \frac{1}{2}\sum_{n=1}^{\infty}\alpha_n^2\cos(2\pi n\Omega\tau), \tag{3.10}$$

we derive formulas for $\mathrm{cov}(n_1(T), n_2(T))$ and $\mathrm{var}(n(T))$. We first follow the derivation in Cox [4] for the formula of the spike count variance. We extend it to spike trains with time varying rates, and relate it to the autocorrelation function. We then apply this same formula to the cross-correlation function to obtain the covariance, and calculate the correlation coefficient of the spike count over a window of size T,

$$\rho(T) = \frac{\mathrm{cov}\{n_1(T), n_2(T)\}}{\mathrm{var}\{n(T)\}}. \tag{3.11}$$

Here, the variances of the spike counts from the two neurons are identical so

$$\mathrm{var}\{n(T)\} = \sqrt{\mathrm{var}\{n_1(T)\}\mathrm{var}\{n_2(T)\}} = \mathrm{var}\{n_1(T)\} = \mathrm{var}\{n_2(T)\}.$$

First, note that the variance of a sum of spike counts over two intervals, A and B, can be broken down into

$$\mathrm{var}\{n(A) + n(B)\} = \mathrm{var}\{n(A)\} + \mathrm{var}\{n(B)\} + 2\mathrm{cov}\{n(A), n(B)\}. \tag{3.12}$$

Let $n(t)$ be the spike count over a window of size t. By the fundamental theorem of calculus, $n(t) = \int_0^t n'(z)dz$, where the integral can be considered as the limit of Riemann sums. Thus,

we can apply the sum rule in Equation (3.12) to obtain

$$\begin{aligned}
\text{var}\{n(t)\} =& \text{var}\left\{\int_0^t n'(z)dz\right\} \\
=& \text{var}\left\{\lim_{k\to\infty}\sum_{j=1}^{k}\frac{t}{k}n'\left(\frac{jt}{k}\right)\right\} \\
=& \lim_{k\to\infty}\sum_{j=1}^{k}\text{var}\left\{\frac{t}{k}n'\left(\frac{jt}{k}\right)\right\} + 2\lim_{k\to\infty}\sum_{j=1}^{k}\sum_{p=1}^{k-j}\text{cov}\left\{\frac{t}{k}n'\left(\frac{jt}{k}\right), \frac{t}{k}n'\left(\frac{(j+p)t}{k}\right)\right\} \\
=& \lim_{k\to\infty}\sum_{j=1}^{k}\text{var}\left\{n'\left(\frac{jt}{k}\right)\right\}\frac{t}{k} + 2\lim_{k\to\infty}\sum_{j=1}^{k}\sum_{p=1}^{k-j}\text{cov}\left\{n'\left(\frac{jt}{k}\right), n'\left(\frac{(j+p)t}{k}\right)\right\}\left(\frac{t}{k}\right)^2.
\end{aligned}$$

Rewriting the sums as integrals we have

$$\text{var}\{n(t)\} = \int_0^t \text{var}\left\{n'(z)\right\}dz + 2\int_0^t\int_0^{t-z}\text{cov}\left\{n'(z), n'(z+u)\right\}dudz. \tag{3.13}$$

We assume that the spiking process is orderly, which means that the probability of having at least two spikes in the interval $(t, t+\epsilon)$ is $o(\epsilon)$. This implies that

$$\begin{aligned}
\text{var}\{n\left(z, z+\epsilon\right)\} =& E[\{n\left(z, z+\epsilon\right)\}^2] - E[n\left(z, z+\epsilon\right)]^2 \\
=& P\left[n(z, z+\epsilon) = 1\right] + o(\epsilon) - P\left[n(z, z+\epsilon) = 1\right]^2 \\
=& \nu\epsilon + o(\epsilon),
\end{aligned}$$

where the expected values are taken with respect to both time and realizations. Similarly, for $u > 0$,

$$\begin{aligned}
\text{cov}\{n\left(z, z+\epsilon_1\right), n\left(z+u, z+u+\epsilon_2\right)\} =& E[n\left(z, z+\epsilon_1\right)n\left(z+u, z+u+\epsilon_2\right)] \\
& - E[n\left(z, z+\epsilon_1\right)]E[n\left(z+u, z+u+\epsilon_2\right)] \\
=& P\left[n(z, z+\epsilon_1) = 1, n(z+u, z+u+\epsilon_2) = 1\right] \\
& - P\left[n(z, z+\epsilon_1) = 1\right]P\left[n(z+u, z+u+\epsilon_2) = 1\right] \\
& + o(\epsilon_1\epsilon_2) \\
=& f_{av}(u)\epsilon_1\epsilon_2 - \nu^2\epsilon_1\epsilon_2 + o(\epsilon_1\epsilon_2).
\end{aligned}$$

Once again, we take the expected values with respect to both time and realizations, so that the probabilities refer to the probability of firing averaged over the phase of the oscillation at time z.

Then using the definition of derivative we have

$$\begin{aligned}\text{var}\{n'(z)\} =& \text{var}\left\{\lim_{\epsilon\to 0}\frac{n(z,z+\epsilon)}{\epsilon}\right\}\\ =& \lim_{\epsilon\to 0}\frac{1}{\epsilon}\text{var}\{n(z,z+\epsilon)\},\end{aligned}$$

and

$$\begin{aligned}\text{cov}\{n'(z),n'(z+u)\} =& \text{cov}\left\{\lim_{\epsilon_1\to 0}\frac{n(z,z+\epsilon_1)}{\epsilon_1},\lim_{\epsilon_2\to 0}\frac{n(z+u,z+u+\epsilon_2)}{\epsilon_2}\right\}\\ =& \lim_{\epsilon_1\to 0}\lim_{\epsilon_2\to 0}\frac{1}{\epsilon_1\epsilon_2}\text{cov}\left\{n(z,z+\epsilon_1),n(z+u,z+u+\epsilon_2)\right\}.\end{aligned}$$

Plugging these into equation 3.13, we obtain

$$\begin{aligned}\text{var}\{n(t)\} =& \int_0^t \lim_{\epsilon\to 0}\frac{1}{\epsilon}\nu\epsilon dz + 2\int_0^t\int_0^{t-z}\lim_{\epsilon_1\to 0}\lim_{\epsilon_2\to 0}\frac{1}{\epsilon_1\epsilon_2}\left[f_{av}(u)-\nu^2\right]\epsilon_1\epsilon_2 du dz\\ =& \int_0^t \nu dz + 2\int_0^t\int_0^{t-z}\left[f_{av}(u)-\nu^2\right]du dz\\ =& \nu t + 2\int_0^t\int_0^{t-u}\left[f_{av}(u)-\nu^2\right]dz du\\ =& \nu t + 2\int_0^t (t-u)\left[f_{av}(u)-\nu^2\right]du\\ =& \int_{-t}^t (t-|u|)\left[\nu\delta(u)+f_{av}(u)-\nu^2\right]du\\ =& \int_{-t}^t (t-|u|)A(u)du,\end{aligned}$$

where the last substitution is from Equation (3.6)

Thus, the variance of the spike count over a finite window of length T is the integral of the autocorrelation function against a weighting factor:

$$\begin{aligned}
\mathrm{var}(n(T)) &= \int_{-T}^{T} A(\tau)(T-|\tau|)d\tau \\
&= \int_{-T}^{T} \left[\alpha_0\delta(\tau) + \frac{1}{2}\sum_{n=1}^{\infty}\alpha_n^2\cos(2\pi n\Omega\tau)\right](T-|\tau|)d\tau \\
&= \int_{-T}^{T} \alpha_0\delta(\tau)(T-|\tau|)d\tau \\
&\quad + \int_{-T}^{0}\left(\frac{1}{2}\sum_{n=1}^{\infty}\alpha_n^2\cos(2\pi n\Omega\tau)\right)(T+\tau)\,d\tau + \int_{0}^{T}\left(\frac{1}{2}\sum_{n=1}^{\infty}\alpha_n^2\cos(2\pi n\Omega\tau)\right)(T-\tau)d\tau \\
&= \alpha_0 T + \frac{1}{2}\sum_{n=1}^{\infty}\alpha_n^2\left[\int_{-T}^{0}\cos(2\pi n\Omega\tau)\,(T+\tau)\,d\tau + \int_{0}^{T}\cos(2\pi n\Omega\tau)\,(T-\tau)\,d\tau\right].
\end{aligned}$$

Then integrating by parts gives

$$\begin{aligned}
\mathrm{var}(n(T)) &= \alpha_0 T + \frac{1}{2}\sum_{n=1}^{\infty}\frac{\alpha_n^2}{2\pi n\Omega}\left[-\int_{-T}^{0}\sin(2\pi n\Omega\tau)d\tau + \int_{0}^{T}\sin(2\pi n\Omega\tau)d\tau\right] \\
&= \alpha_0 T + \frac{1}{2}\sum_{n=1}^{\infty}\left(\frac{\alpha_n}{2\pi n\Omega}\right)^2\left[\cos(2\pi n\Omega\tau)\Big|_{-T}^{0} - \cos(2\pi n\Omega\tau)\Big|_{0}^{T}\right],
\end{aligned}$$

which simplifies to

$$\mathrm{var}(n(T)) = \alpha_0 T + \sum_{n=1}^{\infty}\left(\frac{\alpha_n}{2\pi n\Omega}\right)^2\left[1-\cos(2\pi n\Omega T)\right]. \tag{3.14}$$

Because the two neurons are homogeneous, and their correlation is expected to be symmetric about $\tau = 0$, we can calculate the covariance in the same way, using the cross-correlation function instead of the autocorrelation function:

$$\begin{aligned}
\mathrm{cov}(n_1(T), n_2(T)) &= \int_{-T}^{T} C(\tau)(T-|\tau|)d\tau \\
&= \int_{-T}^{T}\left[c\alpha_0\delta(\tau) + \frac{1}{2}\sum_{n=1}^{\infty}\alpha_n^2\cos(2\pi n\Omega\tau)\right](T-|\tau|)d\tau,
\end{aligned}$$

which simplifies to

$$\mathrm{cov}(n_1(T), n_2(T)) = c\alpha_0 T + \sum_{n=1}^{\infty} \left(\frac{\alpha_n}{2\pi n\Omega}\right)^2 [1 - \cos(2\pi n\Omega T)]\,. \tag{3.15}$$

It is clear that the covariance and variance of the spike counts are the same in all oscillatory terms, since the equation for the cross-correlation function and auto-correlation function are identical, up to the first Fourier coefficient.

Plugging the covariance and variance into Equation 3.11 gives the correlation coefficient,

$$\rho(T) = \frac{c\alpha_0 T + \sum_{n=1}^{\infty} \left(\frac{\alpha_n}{2\pi n\Omega}\right)^2 [1 - \cos(2\pi n\Omega T)]}{\alpha_0 T + \sum_{n=1}^{\infty} \left(\frac{\alpha_n}{2\pi n\Omega}\right)^2 [1 - \cos(2\pi n\Omega T)]}. \tag{3.16}$$

It is clear from Equation (3.16) that the rhythms seen in the correlation coefficient are due to a difference in the covariance and variance of spike emission, rather than in long time-scale oscillations, since the only difference between the numerator and denominator is the first Fourier coefficient. This is because the oscillations in $\alpha(t)$ are perfectly correlated between the two neurons, which makes the oscillatory terms in the covariance and variance identical. If the oscillations were instead only partially correlated, with a parameter $\tilde{c}$, we would expect that for a critical value, $\tilde{c}^*$, of oscillation correlation, the factor in front of each term of the covariance when compared to the variance would be the same, and the oscillation in the two quantities would cancel out in the ratio.

We test this hypothesis by decorrelating the well heights, and hence the Arrhenius escape rates, in the reduced model. We do this by setting the escape rates, $\alpha_1(t)$ and $\alpha_2(t)$, of the two neurons to be identical in a proportion $\tilde{c}$ of the trials, while in the rest of the trials the phases at which the well-height oscillations begin is independent. Thus, when we average over trials, the correlation of the rate modulations depends on $\tilde{c}$. We also include spike correlations as before, so the trials in which the escape rates are identical follow the same well-hopping scheme as shown in Figure 14. The trials in which the well-hopping is independent follow the well-hopping schematic shown in Figure 16.

We show numerically that by fixing c and lowering $\tilde{c}$, the oscillation of the correlation coefficient decreases toward zero and eventually switches direction, as seen in Figure 17. Assuming that the relationship is continuous, this means that there must be a critical value,

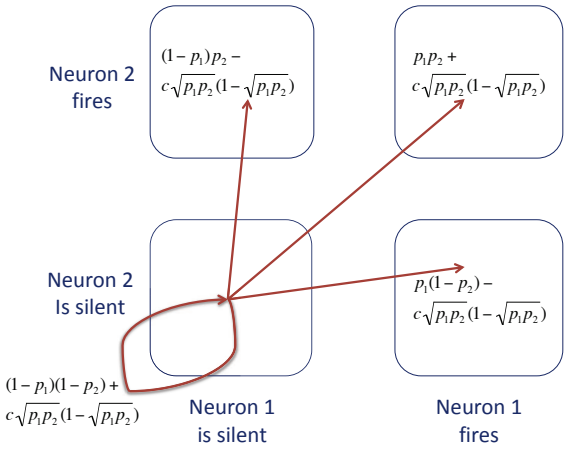

Figure 16: **Joint escape probabilities for two neurons with independent rate modulations in the interval** $(t, t+dt)$**.** The neurons have independent escape probabilities $p_1(t)$ and $p_2(t)$ and spike correlation c. This schematic shows the joint escape probabilities used for the proportion $1-\tilde{c}$ of the trials that use independent rates.

$\tilde{c}^*$, which depends on c and for which the oscillation disappears. This indicates that the oscillations seen in the correlation coefficient in this work will be present for nearly all combinations of c and $\tilde{c}$. In fact, because the equation for $\rho(T)$ holds for any periodic modulation of the well-height, this indicates that in general, periodic inputs will lead to oscillations in the output correlation coefficient, unless the spike time correlation and correlation of the rate modulations are perfectly balanced. This effect causes the correlations in a system with oscillatory inputs to be very sensitive to time-scale.

3.4 COMPARISON WITH COMPUTATIONAL RESULTS

Now that we have an analytic expression for the correlation coefficient of the reduced model, we can investigate how this compares with and gives insight into the behavior of $\rho_{\text{out}}(T)$ in the computational model. In Figure 18 the output correlation coefficients of the computational

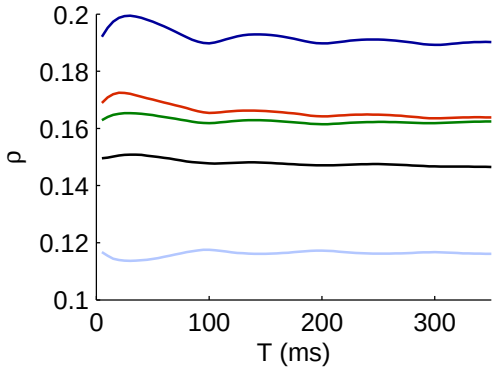

Figure 17: **Effects of decorrelating well height oscillations.** Numerically calculated $\rho(T)$ from simulations of the reduced model with $c = 0.3$ for different values of $\tilde{c}$. Dark blue: $\tilde{c} = 0.4$, Red: $\tilde{c} = 0.3$, Green: $\tilde{c} = 0.2$, Black: $\tilde{c} = 0.1$, Light blue: $\tilde{c} = 0$.

models are plotted alongside the analytically calculated $\rho(T)$ of the reduced model for two different values of c. Figure 18 A plots the correlation coefficients calculated when $c = 0$, while Figure 18 B plots the correlation coefficients calculated for $c = 0.2$ in the computational models, and for $c = 0.08$ in the reduced model. For the computational model simulations, we simplify the non-bursty oscillatory inputs from GPi by using only a single sine wave instead of a sum of sine waves to set the GPi firing rate. We also simplify the oscillatory bursts in GPi by making the variances of the waiting time between bursts and of the burst duration to be zero.

On the left, ρ_{out} is plotted for oscillatory inputs, while on the right we use oscillatory bursts in the inputs. Both oscillatory inputs and oscillatory bursts in the inputs show an oscillation in ρ_{out}, but the amplitude of this oscillation is much higher for the case of oscillatory bursts. This is because in the computational models, the oscillatory bursts with no variability in the inter-burst-intervals cause a very strong dependence of correlation transfer on time-scale. Introducing variability in the timing of the bursts for this case would cause the oscillations in $\rho_{out}(T)$ to have a smaller amplitude and dampen more quickly.

Quantitatively, we do not expect the correlation coefficients to match identically, as even when comparing the conductance-based model and the IFB model, the quantitative results

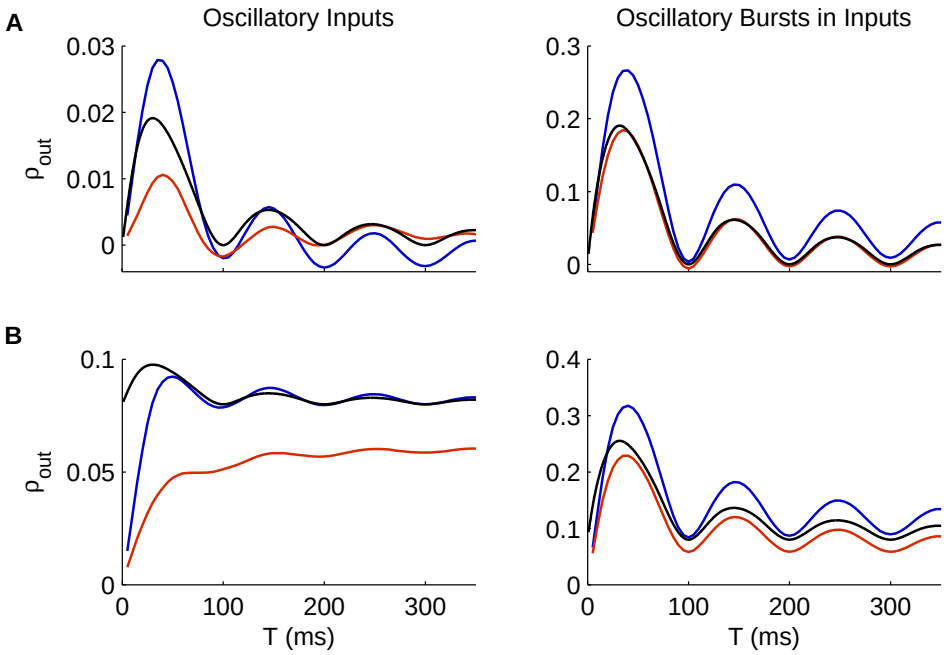

Figure 18: **Oscillations of ρ from reduced model calculations match those in $\rho_{\mathbf{out}}$ from full model simulations.** Correlation coefficient of reduced model (black), conductance-based model (blue), and IFB model (red) of thalamic neurons receiving non-bursty oscillatory inputs (left) and oscillatory bursts in the inputs (right) from GPi, with oscillations at a frequency of 10 Hz. Parameters for reduced model are $D = .1$, $U_0 = 1$, and $\eta = .4$ for oscillatory inputs and $D = .35$, $U_0 = 1$, and $\eta = 1$ for oscillatory bursts. **A.** $c = 0$ **B.** $c = .2$ in the computational models, and $c = .08$ in the reduced model.

for correlation transfer differ in the two systems. The difference between the reduced model prediction and the computational model results is especially large at small window-sizes. This is because the instantaneous correlation level for the reduced model is c (obtained by taking $\lim_{T\to 0}\rho(T)$). In other words, the reduced model assumes the spike correlations are perfectly transferred from input to output. In the full computational models, however, the spike correlations in the inputs do not directly translate into instantaneous correlations in the outputs because of the membrane dynamics of the thalamic models. Also, the refractory period of the computational models will affect correlation transfer on short timescales, while the reduced model has no refractory period. A quantitative difference between the reduced model and the computational models is also evident on longer time-scales, because the reduced model assumes perfect correlation transfer since it is poisson, while the long time correlations in the computational models are diluted by the non-linearity of the models.

Despite the quantitative differences, the reduced model sheds light on the qualitative behaviors of the correlation coefficient. In particular, the analysis of the reduced model gives insight into the origin and nature of the rhythms seen in $\rho_{\text{out}}(T)$. In the computational models, we observed that the time between peaks of $\rho_{\text{out}}(T)$ is equal to the period of the oscillation in the GPi firing rate. This observation is supported by the reduced model, where frequency of the cosine in the correlation coefficient in Equation 3.16 is calculated to be the same as the frequency of the well modulation. Thus, the frequency of the oscillation in GPi determines the time scales on which the thalamic neurons will be most correlated. Also, from Equation 3.16, it is clear that as $T \to \infty$, the oscillations in $\rho_{\text{out}}(T)$ dampen, and ρ_{out} asymptotes to a constant value. This effect is seen in the correlation susceptibility of the computational models, in Figures 9 and 11.

Finally, as discussed in Section 3.3, rhythms in the correlation coefficient are present despite identical inhibitory input rate modulations, due to differences in the covariance and variance of spike emission. Varying the input rate correlations shows that very specific matching between input rate correlations and spike time correlations would be necessary to get rid of these rhythms. This indicates that the oscillations seen in $\rho_{\text{out}}(T)$ in the computational models are robust to changes in parameters.

4.0 CONCLUSIONS

We have shown that firing patterns in GPi which have been observed experimentally under parkinsonian conditions do indeed affect the correlation in the GPi as well as the way that correlations are transferred from the basal ganglia to thalamus. This conclusion is supported by our computational model simulations as well as by the reduced model calculations. A summary of the main results from this work which support this conclusion is shown in Table 2.

In our models, shared oscillations in the firing rates of GPi spike trains are sufficient to cause a peak in their cross-spectrum. Thus, if the firing rates of the neurons in basal ganglia were oscillating together due to some global modulation, then the correlations as measured by the cross-correlation function or by the cross-spectrum would be increased, as is reported in experiments. At time scales corresponding the to the period of the oscillation in the firing rate, the spike counts from GPi are more correlated when the firing rate is non-homogeneous than when it is constant, even when the instantaneous correlation, c, is the same. Our reduced point process model shows that this effect is very robust to changes in parameters, and is apparent for almost all combinations of spike and rate correlations. Thus, the experimentally reported increases in correlations in GPi could be due to global oscillations in firing rate, as well as increased spike correlations.

By looking at correlation susceptibility as a measure of correlation transfer, we can see how well the correlations seen in GPi are transferred to thalamus under the different firing patterns, regardless of the level of correlation in GPi. Our computational models show that patterns of input firing that include bursts of spikes cause the system to be much more susceptible to passing along correlations. Thus, the models predict that a small change in correlations in GPi will cause a larger change in thalamic correlation when the inputs from

Table 2: Summary of results.

Main Results	**Figures**	**Equations**
Bursty inputs cause increased correlation susceptibility	9	
Oscillatory inputs cause output correlation susceptibility to be oscillatory with respect to time-scale of observation	9	
Susceptibility decreases as oscillation amplitude increases	10	
Susceptibility increases as oscillation frequency decreases	11	
Removing T-current affects firing properties but has little effect on correlation susceptibility	13	
Frequency of rhythm in output correlation coefficient is same as frequency of input rate modulation	18	3.16
Rhythm in correlation coefficient is due to differences in covariance and variance of spike emission	7	3.9, 3.10, 3.14, 3.15, 3.16

GPi are bursty than when the inputs are either purely oscillatory or of constant rate. This effect could be due to the sharp changes in firing rate that occur when the GPi fires a burst. Such large, fast changes are a strongly inhomogeneous signal to both neurons, which may make them more sensitive to small changes in the proportion of shared input spikes.

We also show that the correlation susceptibility and ρ_{out} are both affected by the time scale of the oscillations in the GPi firing rates. In particular, when two neurons receive identical rate modulations in their inputs, correlations are maximized on a time scale of half the period of the firing rate oscillation. The analysis of our reduced model shows that differences in the covariance and variance of spike timing are sufficient to cause this dependency of the correlations on timescale. It also indicates that the rhythmicity in the correlation coefficient with respect to window size for neurons with correlated oscillatory rates is very robust. This non-monotonic dependency of correlation on the window size points to the critical importance of the observation window used when measuring spike count correlations.

Also of interest is how this model could give insight into the mechanism by which deep brain stimulation (DBS) is effective. The computational models suggest that increasing the frequency of the oscillations in GPi decreases the strength of the oscillation seen in the correlation susceptibility. Also, increasing the amplitude of non-bursty oscillations in GPi decreases the correlation susceptibility of the system. Taken together, these two effects may mean that DBS at high frequencies could effectively decrease the amount of correlations being passed from GPi to the thalamus. If these correlations are indicative of a pathological breakdown of pathway segregation, reducing correlation transfer may contribute to the positive effect of DBS.

We also showed that although the T-current in the TC neurons affects the pattern of spiking, and the type of inputs that lead to a spike, it does not have a large effect on the transfer of correlations through the system. In particular, the reduced model includes no T-current, yet it still produces results that are qualitatively very similar to the computational models. Also, removing the T-current in the computational models shows little effect on correlation susceptibility. Since it has been shown that T-current bursts may not be a prominent feature of thalamic activity in non-tremor parkinsonism [19], but may be more prominent during

tremor, the lack of influence of the T-current on correlation transfer indicates that it may be similarly affected both in tremor and non-tremor periods.

In parkinsonian conditions, increased correlations in basal ganglia are thought to be a pathological breakdown of functional circuit segregation [3, 18]. Other work has posited that increased correlations seen in the thalamus in parkinsonian conditions is indicative of this circuit desegregation [19]. Our work shows that the increase in correlations in the thalamus may be due to a dual effect of increased correlations in basal ganglia as well as increased correlation susceptibility because of bursty GPi firing patterns. Such an increase in correlation susceptibility would make thalamic neurons very sensitive to even small fluctuations in correlations in GPi. This effect could be compounded by the sensitivity of correlations to the time-scale of oscillations in the GPi activity levels. This increased correlation in the thalamus may be detrimental to the ability of the thalamus to accurately relay excitatory information it receives from cortex and may also have added downstream effects since the information relayed through the thalamus is critical to motor control.

APPENDIX

CALCULATIONS OF FOURIER COEFFICIENTS

A.1 SINUSOIDAL WELL

We assume here that the depth of the energy well from which a neuron must escape to fire is sinusoidally rocked by the sinusoidally modulated input with frequency Ω,

$$U(t) = U_0 \left(1 - \eta \cos\left(2\pi\Omega t\right)\right),$$

so the Arrhenius rate of escape is given by

$$\alpha(t) = \beta \exp\left[-\frac{U_0}{D}\left(1 - \eta \cos\left(2\pi\Omega t\right)\right)\right],$$

as in Wiesenfeld et al [30]. Since $M = \frac{1}{\Omega}$, this is M-periodic and even, so can be expanded into a Fourier series of the form

$$\alpha(t) = \alpha_0 + \sum_{n=1}^{\infty} \alpha_n \cos\left(2\pi n\Omega t\right).$$

The coefficients of this series are given by

$$\begin{aligned}\alpha_0 =& \frac{1}{M} \int_{-\frac{M}{2}}^{\frac{M}{2}} \alpha(t)dt \\ =& \frac{\beta}{M} e^{-\frac{U_0}{D}} \int_{-\frac{M}{2}}^{\frac{M}{2}} \exp\left[\frac{\eta U_0}{D}\cos\left(2\pi\Omega t\right)\right] dt.\end{aligned}$$

Letting $\theta = 2\pi\Omega t$, this becomes

$$\begin{aligned}
\alpha_0 =& \frac{\beta}{2\pi} e^{-\frac{U_0}{D}} \int_{-\pi}^{\pi} \exp\left[\frac{\eta U_0}{D}\cos(\theta)\right] d\theta \\
=& \frac{\beta}{\pi} e^{-\frac{U_0}{D}} \int_{0}^{\pi} \exp\left[\frac{\eta U_0}{D}\cos(\theta)\right] d\theta \\
=& \beta e^{-\frac{U_0}{D}} I_0\left(\frac{\eta U_0}{D}\right)
\end{aligned}$$

and for $n \geq 1$,

$$\begin{aligned}
\alpha_n =& \frac{2}{M} \int_{-\frac{M}{2}}^{\frac{M}{2}} \alpha(t)\cos\left(2\pi n\Omega t\right) dt \\
=& \frac{2\beta}{M} e^{-\frac{U_0}{D}} \int_{-\frac{M}{2}}^{\frac{M}{2}} \exp\left[\frac{\eta U_0}{D}\cos\left(2\pi\Omega t\right)\right]\cos\left(2\pi n\Omega t\right) dt \\
=& \frac{\beta}{\pi} e^{-\frac{U_0}{D}} \int_{-\pi}^{\pi} \exp\left[\frac{\eta U_0}{D}\cos(\theta)\right]\cos\left(n\theta\right) dt \\
=& \frac{2\beta}{\pi} e^{-\frac{U_0}{D}} \int_{0}^{\pi} \exp\left[\frac{\eta U_0}{D}\cos(\theta)\right]\cos\left(n\theta\right) dt \\
=& 2\beta e^{-\frac{U_0}{D}} I_n\left(\frac{\eta U_0}{D}\right)
\end{aligned}$$

where

$$I_n(z) = \frac{1}{\pi}\int_0^{\pi} e^{z\cos(\theta)}\cos(n\theta)d\theta$$

is the modified Bessel function of order n, for $n = 0, 1, 2, ...$

In summary,

$$\alpha_0 = \beta e^{-\frac{U_0}{D}} I_0\left(\frac{\eta U_0}{D}\right)$$

and

$$\alpha_j = 2\beta e^{-\frac{U_0}{D}} I_j\left(\frac{\eta U_0}{D}\right)$$

for $j \geq 1$.

A.2 STEP FUNCTION WELL

Here, the depth of the energy well from which a neuron must escape in order to fire is assumed to be modulated by the periodic step function,

$$U(t) = U_0 \left(1 + \eta H \left[t\text{mod}(M) - \frac{T_1}{2}\right] H \left[\frac{T_1}{2} + T_2 - t\text{mod}(M)\right]\right).$$

The well is assumed to be at its baseline depth for time T_1, and then is transiently set to a new depth for time T_2. Then $M = T_1 + T_2$ is the period of the oscillation, and the Arrhenius rate of escape is given by

$$\alpha(t) = \beta \exp\left[-\frac{U_0}{D}\left(1 + \eta H \left[t\text{mod}(M) - \frac{T_1}{2}\right] H \left[\frac{T_1}{2} + T_2 - t\text{mod}(M)\right]\right)\right],$$

This rate is an M-periodic, even function, so it can also be expanded into a fourier series of the form

$$\alpha(t) = \alpha_0 + \sum_{j=1}^{\infty} \alpha_j \cos\left(\frac{2\pi j t}{M}\right).$$

Thus, we have,

$$\begin{aligned}
\alpha_0 =& \frac{\beta}{M} e^{-\frac{U_0}{D}} \int_0^M \exp\left[-\frac{\eta U_0}{D} H \left[t\text{mod}(M) - \frac{T_1}{2}\right] H \left[\frac{T_1}{2} + T_2 - t\text{mod}(M)\right]\right] dt \\
=& \frac{\beta}{M} e^{-\frac{U_0}{D}} \left[\frac{T_1}{2} + \int_{\frac{T_1}{2}}^{\frac{T_1}{2}+T_2} e^{-\frac{\eta U_0}{D}} dt + M - \left(\frac{T_1}{2} + T_2\right)\right] \\
=& \frac{\beta}{M} e^{-\frac{U_0}{D}} \left[T_1 + T_2 e^{-\frac{\eta U_0}{D}}\right],
\end{aligned}$$

where the last equality uses the fact that $M = T_1 + T_2$. Similarly, for $j \geq 1$

$$\begin{aligned}
\alpha_j =& \frac{2\beta}{M} e^{-\frac{U_0}{D}} \int_{-\frac{M}{2}}^{\frac{M}{2}} \exp\left[-\frac{\eta U_0}{D} H \left[t\text{mod}(M) - \frac{T_1}{2}\right] H \left[\frac{T_1}{2} + T_2 - t\text{mod}(M)\right]\right] \cos\left(\frac{2\pi j t}{M}\right) dt \\
=& \frac{2\beta}{M} e^{-\frac{U_0}{D}} \left[\int_{-\frac{M}{2}}^{-\frac{T_1}{2}} e^{-\frac{\eta U_0}{D}} \cos\left(\frac{2\pi j t}{M}\right) dt + \int_{-\frac{T_1}{2}}^{\frac{T_1}{2}} \cos\left(\frac{2\pi j t}{M}\right) dt + \int_{\frac{T_1}{2}}^{\frac{M}{2}} e^{-\frac{\eta U}{D}} \cos\left(\frac{2\pi j t}{M}\right) dt\right] \\
=& \frac{2\beta}{\pi j} e^{-\frac{U_0}{D}} \left(e^{-\frac{\eta U_0}{D}} - 1\right) \sin\left(\frac{\pi j T_1}{M}\right).
\end{aligned}$$

BIBLIOGRAPHY

[1] Chronux software package. http://chronux.org/.

[2] G. E. Alexander and M. D. Crutcher, *Function architecture of basal ganglia circuits: neural substrates of parallel processing*, Trends in Neuronsciences **13** (1990), no. 7, 266–271.

[3] H. Bergman, A. Feingold, A. Nini, A. Raz, H. Slovin, M. Abeles, and E. Vaadia, *Physiological aspects of information processing in the basal ganglia of normal and parkinsonian primates*, Trends in Neurosciences **21** (1998), 32–38.

[4] D. R. Cox and V. Isham, *Point processes*, London: Chapman & Hall, 1980.

[5] P. Dayan and L. F. Abbott, *Theoretical neuroscience: Computational and mathematical modeling of neural systems*, MIT Press, 2001.

[6] J. de la Rocha, B. Doiron, E. Shea-Brown, K. Josic, and A. Reyes, *Correlation between neural spike trains increases with firing rate*, Nature **448** (2007), 802–806.

[7] J. T. Gale, R. Amirnovin, Z. M. Williams, A. W. Flaherty, and E. N. Eskandar, *From symphony to cacophony: Pathophysiology of the human basal ganglia in Parkinson disease*, Neuroscience and Biobehavioral Reviews **32** (2008), 378–387.

[8] C. W. Gardiner, *Handbook of stochastic methods*, Springer, 1985.

[9] J. A. Goldberg, U. Rokni, T. Boraud, E. Vaadia, and H. Bergman, *Spike synchronization in the cortex-basal ganglia networks of parkinsonian primates reflects global dynamics of the local field potentials*, The Journal of Neuroscience **24** (2004), no. 25, 6003–6010.

[10] Y. Guo, J. E. Rubin, C. C. McIntyre, J. L. Vitek, and D. Terman, *Thalamocortical relay fidelity varies across subthalamic nucleus deep brain stimulation protocols in a data-driven computational model*, Journal of Neurophysiology **99** (2008), 1477–1492.

[11] P. Hanggi, P. Talkner, and M. Borkovec, *Reaction-rate theory: Fifty years after Kramers*, Reviews of Modern Physics **62** (1990), no. 2.

[12] G. Heimer, M. Rivlin-Etzion, I. Bar-Gad, J. A. Goldberg, S. N. Haber, and H. Bergman, *Dopamine replacement therapy does not restore the full spectrum of normal pallidal*

activity in the 1-methyl-4-phenyl-1,2,3,6-tetra-hydropyridine primate model, The Journal of Neuroscience **26** (2006), no. 31, 8101–8114.

[13] A. L. Hodgkin and A. F. Huxley, *The dual effect of membrane potential on sodium conductance in the giant axon of Loligo*, Journal of Physiology **116** (1952), 497–506.

[14] P. Jung, *Stochastic resonance and optimal design of threshold detectors*, Physics Letters A **207** (1995), 93–104.

[15] R.E. Kass and V. Ventura, *Spike count correlation increases with length of time interval in the presence of trial-to-trial variation*, Neural Computation **18** (2006), 2583–3591.

[16] P. Mitra and H. Bokil, *Observed brain dynamics*, Oxford University Press, New York, 2008.

[17] G. F. Molnar, A. Pilliar, A. M. Lozano, and J. O. Dostrovsky, *Differences in neuronal firing rates in pallidal and cerebellar receiving areas of thalamus in patients with parkinson's disease, essential tremor, and pain*, Journal of Neurophysiology **93** (2004), 3094 – 3101.

[18] A. Nini, A. Feingold, H. Slovin, and H. Bergman, *Neurons in the globus pallidus do not show correlated activity in the normal monkey, but phase-locked oscillations appear in the MPTP model of parkinsonism*, Journal of Neurophysiology **74** (1995), no. 4, 1800–1805.

[19] M. Pessiglione, D. Guehl, A. Rolland, C. Francois, E. C. Hirsch, J. Feger, and L. Temblay, *Thalamic neuronal activity in dopamine-depleted primates: Evidence for a loss of functional segregation within basal ganglia circuits*, The Journal of Neuroscience **25** (2005), no. 6, 1523–1531.

[20] H. E. Plesser and W. Gerstner, *Noise in integrate-and-fire neurons: from stochastic input to escape rates*, Neural Computation **12** (2000), 367–384.

[21] A. Raz, E. Vaadia, and H. Bergman, *Firing patterns and correlations of spontaneous discharge of pallidal neurons in the normal and the tremulous 1-methyl-4-phenyl-1,2,3,6-tetrahydropyridine vervet model of parkinsonism*, The Journal of Neuroscience **20** (2000), no. 22, 8559 – 8571.

[22] J. Rinzel, *Excitation dynamics: insights from simplified membrane models*, Fed. Proc. **44** (1985), 2944–2946.

[23] M. Rivlin-Etzion, O. Marmor, G. Saban, B. Rosin, S. N. Haber, E. Vaadia, Y. Prut, and H. Bergman, *Low-pass filter properties of basal ganglia-cortical-muscle loops in the normal and MPTP primate model of parkinsonism*, The Journal of Neuroscience **28** (2008), no. 3, 633–649.

[24] J. E. Rubin and D. Terman, *High frequency stimulation of the subthalamic nucleus eliminates pathological thalamic rhythmicity in a computational model*, Journal of Computational Neuroscience **16** (2004), 211–235.

[25] E. Shea-Brown, K. Josic, J. de la Rocha, and B. Doiron, *Correlation and synchrony transfer in integrate-and-fire neurons: Basic properties and consequences for coding*, Physical Review Letters **100** (2008), no. 3.

[26] G. D. Smith, C. L. Cox, S. M. Sherman, and J. Rinzel, *Fourier analysis of sinusoidally driven thalamocortical relay neurons and a minimal integrate-and-fire-or-burst model*, Journal of Neurophysiology **83** (2000), 588–610.

[27] N. G. van Kampen, *Stochastic processes in physics and chemistry*, 2nd ed., Amsterdam: North Holland, 1992.

[28] T. Wichmann, H. Bergman, P. A. Starr, T. Subramanian, R. L. Watts, and M. R. DeLong, *Comparison of MPTP-induced changes in spontaneous neuronal discharge in the internal pallidal segment and in the substantia nigra pars reticula in primates*, Experimental Brain Research **125** (1999), 397–409.

[29] T. Wichmann and J. Soares, *Neuronal firing before and after burst discharges in the monkey basal ganglia is predictably patterned in the normal state and altered in parkinsonism*, Journal of Neurophysiology **95** (2006), 2120 – 2133.

[30] K. Wiesenfeld, D. Pierson, E. Pantazelou, C. Dames, and F. Moss, *Stochastic resonance on a circle*, Physical Review Letters **72** (1994), no. 14, 2125–2129.